

AD-A103 435

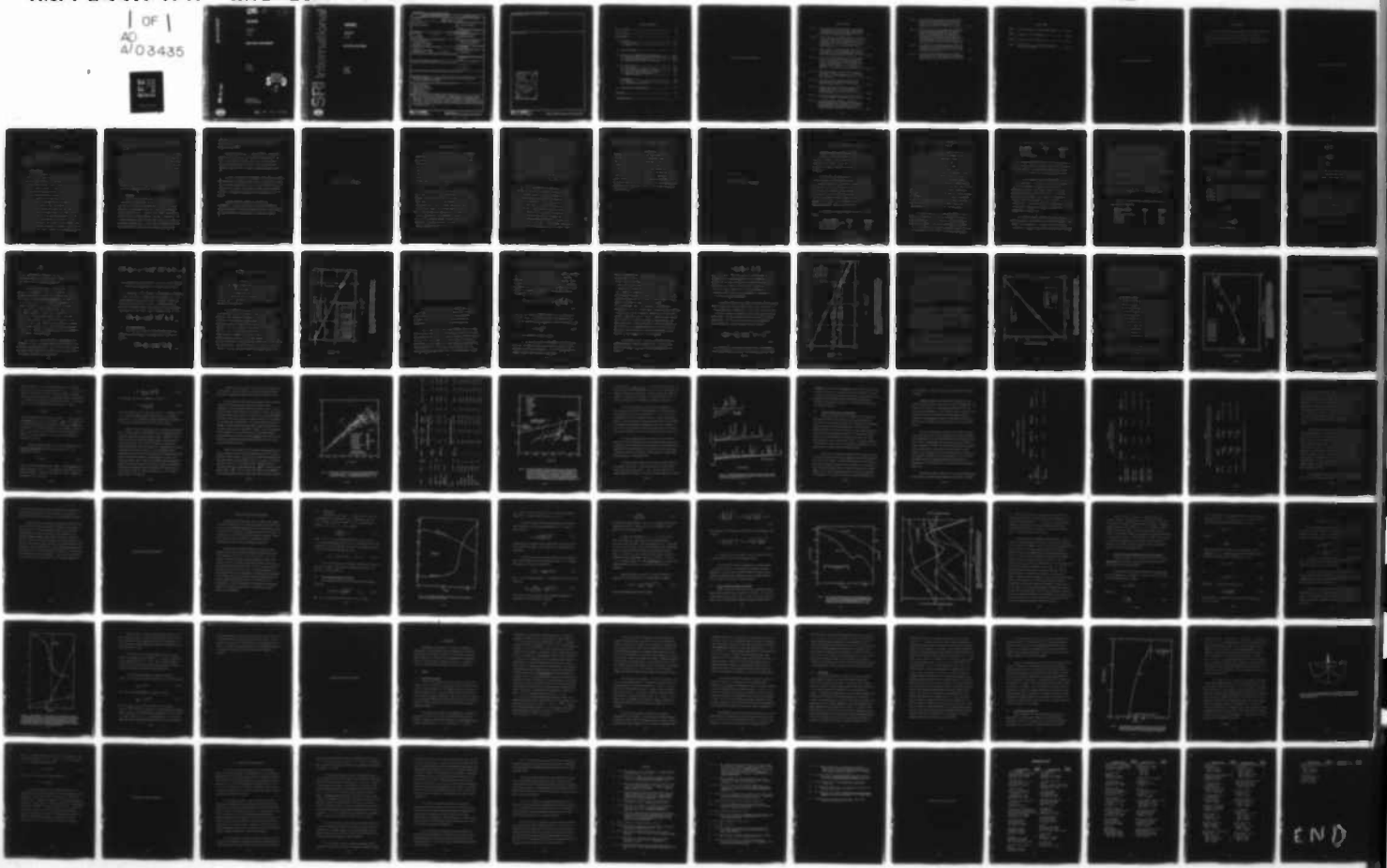
SRI INTERNATIONAL ARLINGTON VA
NUCLEAR CRATERING. (U)
JUN 80 H M FOLEY, J I KATZ, W H PRESS
SRI-JSR-79-09

INCI ACCEPTED

1 OF 1
AO
4/03435

F/G 18/3

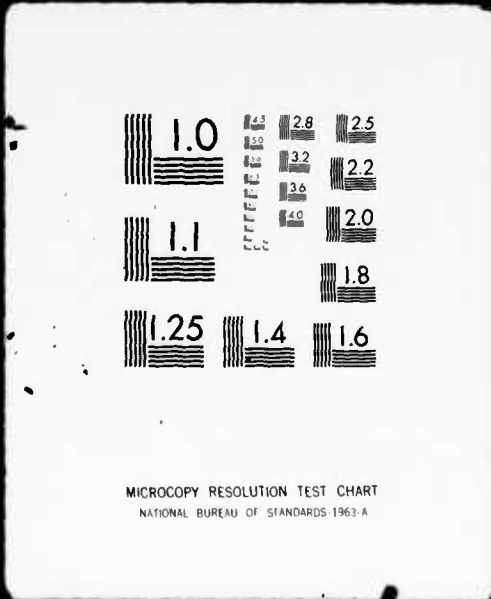
DNA001-75-C-0121
NL



SECRET

| OF |

AD
A/03435



AD A103435

LEVEL

17

(2) fm

JASON

Technical Report
JSR-79-09

June 1980

NUCLEAR CRATERING

H. M. Foley
J. I. Katz
W. H. Press
J. D. Sullivan

DTIC
ELECTED
AUG 28 1981
S D

H
ls

SRI International
1611 North Kent Street
Arlington, Virginia 22209



80 8 28 028

sri



sri international

JASON

Technical Report
JSR-79-09

June 1980

NUCLEAR CRATERING

H. M. Foley
J. I. Katz
W. H. Press
J. D. Sullivan

~~INCLASSIFIED~~

SECURITY CLASSIFICATION OF THIS PAGE (When Data Entered)

REPORT DOCUMENTATION PAGE		READ INSTRUCTIONS BEFORE COMPLETING FORM
1. REPRT NUMBER JSR-79-09	2. GOVT ACCESSION NO <i>AD-A103</i>	3. RECIPIENTS CATALOG NUMBER <i>435</i>
4. TITLE (and Subtitle) <i>NUCLEAR CRATERING</i>	5. TYPE OF REPRT & PERIOD COVERED <i>Technical Report.</i>	
7. AUTHORIS: H. M. Foley J. I. Katz W. H. Press	14. CONTROLLING OFFICE NAME AND ADDRESS Director Defense Nuclear Agency Washington, D.C. 20305	6. PERFORMING ORG REPORT NUMBER <i>JSR-79-09</i>
9. PERFDMING ORGANIZATION NAME AND ADDRESS SRI International 1611 North Kent Street Arlington, VA 22209	10. PROGRAM ELEMENT, PROJECT, TASK AREA & WORK UNIT NUMBERS <i>Subtask K43AAX4X907-15</i>	
11. CDNTROLLING OFFICE NAME AND ADDRESS	12. REPORT DATE <i>June 1980</i>	13. NO. OF PAGES
14. MONITORING AGENCY NAME & ADDRESS (if diff. from Controlling Office)	15. SECURITY CLASS. (of this report) <i>UNCLASSIFIED</i>	
16. DISTRIBUTION STATEMENT (of this report) Approved for public release; distribution unlimited.	16. DECLASSIFICATION/DOWNGRADING SCHEDULE <i>N/A</i>	
17. DISTRIBUTION STATEMENT (of the abstract entered in Block 20, if different from report)	(16) K43AAXY (17) X907	
18. SUPPLEMENTARY NOTES This work sponsored by the Defense Nuclear Agency under RDT&E RMSS Code B337075462 K43AAX4X90715 H2590D.		
19. KEY WORDS (Continue on reverse side if necessary and identify by block number) Nuclear Cratering Early Time Processes Nuclear Surface Bursts Scaling Laws Radiation Coupling		
20. ABSTRACT (Continue on reverse side if necessary and identify by block number) This report describes an investigation of crater formation by nuclear surface bursts; early time processes (radiation and hydrodynamics) and scaling laws are emphasized. We have not attempted a complete theoretical or experimental review of nuclear cratering. Rather this report is intended to be a simple presentation of the important physical processes involved in cratering along with their spatial and temporal scales.		

SECURITY CLASSIFICATION OF THIS PAGE (When Data Entered)

19 KEY WORDS (Continued)

20 ABSTRACT (Continued)

Accession For	
NTIS GRA&I	<input type="checkbox"/>
DTIC TAB	<input type="checkbox"/>
Unannounced	<input type="checkbox"/>
Justification _____	
By _____	
Distribution/ _____	
Availability Codes	
Avail and/or	
Dist	Special
A	

DD FORM 1 JAN 73 1473 (BACK)

EDITION OF 1 NOV 65 IS OBSOLETE

SECURITY CLASSIFICATION OF THIS PAGE (When Data Entered)

TABLE OF CONTENTS

LIST OF FIGURES.....	vii
LIST OF TABLES.....	ix
ACKNOWLEDGMENTS.....	x1
I. INTRODUCTION.....	I-1
1.1 General Remarks.....	I-1
1.2 Contents.....	I-2
II. PHYSICAL PHENOMENA.....	II-1
III. THEORETICAL AND PHENOMENOLOGICAL SCALING LAWS.....	III-1
3.1 Dimensional Analysis and Centrifuge Scaling Laws....	III-1
3.2 Phenomenological Scaling Laws.....	III-20
3.3 Comparison between Theory and Experiment.....	III-29
IV. RADIATIVE COUPLING.....	IV-1
4.1 Source Model.....	IV-2
4.2 Ground Opacity and Radiative Transfer.....	IV-2
4.3 Energy and Impulse Coupled to the Ground.....	IV-6
4.4 Competition Between Hydrodynamics and Radiation Diffusion.....	IV-10
V. HYDRODYNAMICS.....	V-1
5.1 Blowoff.....	V-1
5.2 Incompressible Hydrodynamics.....	V-7
VI. CONCLUSIONS AND RECOMMENDATIONS.....	VI-1
REFERENCES.....	R-1
DISTRIBUTION LIST.....	D-1

This page left blank intentionally

LIST OF FIGURES

- Fig. 3.1 Crater volumes vs gravity strength for zero height of burst HE shots over Ottawa sand. Note the high reproducibility of the crater volumes under these well controlled laboratory situations..... III-10
- Fig. 3.2 Crater volumes at zero height of burst as a function of gravity scaled yield for various soils. The curves correspond to the formula developed in ref. 6 and reproduced as Eq. (3.16) of this report. The ranges indicated at the top of the figure correspond to normal gravity..... III-15
- Fig. 3.3 Crater volume vs yield (equivalently mass) for TNT at zero height of burst over alluvium. The curve corresponds to Eq. (3.16) with parameters determined entirely by centrifuge crater studies..... III-17
- Fig. 3.4 The trend of crater aspect ratio r/d with crater depth d for surface and near surface bursts for nuclear and HE sources at normal gravity and HE craters at enhanced gravity. The centrifuge crater depths have been scaled by g as required by similarity. The centrifuge cratering medium was wet sand..... III-19
- Fig. 3.5 The height of burst curve for HE (all geologies) normalized according to $\phi_{HE}(0) = 1$. Also shown are values of the "HE cratering efficiency" n for generic sources..... III-24
- Fig. 3.6 The height of burst curves for radiating (high energy density) and non-radiating (low energy density) nuclear sources..... III-26
- Fig. 3.7 Averaged cross sections through HE and HE craters formed in PPG coral. Note the progressive flattening (increase in aspect ratio) as crater size increases..... III-28
- Fig. 4.1 The time and temperature functions for the standard 1 MT nuclear source used in this section..... IV-3
- Fig. 4.2 The fireball depth of heating ℓ vs radius r predicted by Eq. (4.8). Also shown for convenience is the temperature curve from Fig. 4.1. For the reasons discussed in the text the model does not properly treat the region $2 \text{ m} < r < 20 \text{ m}$ IV-7

- Fig. 4.3 Energy and momentum coupled to the ground according to the fireball coupling model of this section. Curves for the integrated contributions with and without the questionable intermediate region are shown..... IV-8
- Fig. 4.4 The "trajectory" of the radiation-ground coupling problem in temperature-time space. In region (B) radiation diffuses many mean free paths before source turnoff, hydrodynamics is negligible. In (C) radiation diffuses many mean free paths but hydrodynamic motion catches up before source turnoff. In (D) hydrodynamic motion occurs before ground material has been heated to the source temperature.. IV-13
- Fig. 5.1 Contributions to the momentum impulse given to the ground from the radiation induced vacuum blow off described in the preceding sections and the airslap discussed in this section..... V-8
- Fig. 5.2 The initial downward impulse transferred to the ground spreads over a widening area by hydrodynamic motion which is well approximated by incompressible flow..... V-10

LIST OF TABLES

TABLE I	Crater Parameters for Nuclear Surface Bursts.....	III-25
TABLE II	Comparison of Crater Dimensions.....	III-31
TABLE III	Comparison of Crater Dimensions.....	III-32
TABLE IV	Code Predictions for 5.0 MT Radiating Nuclear Burst at 1.0 m Height.....	III-33

This page left blank intentionally

ACKNOWLEDGMENTS

The authors wish to thank the many members of the cratering community who were helpful during the course of this study. We especially acknowledge helpful conversations with Skip Knowles, Bud Pyatt, Bob Allen, Gerry Nutt, Bob Schmidt, Keith Holsapple, Gene Sevin, Dave Spangler and Bob Swedock.

This page left blank intentionally

I INTRODUCTION

This report describes the results of an investigation of crater formation by nuclear surface bursts done during the 1978 and 1979 JASON Summer Studies. Early time processes (radiation and hydrodynamics) and scaling laws are emphasized.

1.1 General Remarks

Before discussing in detail the contents of this report, let us first make clear the spirit in which this work is presented. We have not attempted a complete theoretical or experimental review of the nuclear cratering problem; nor have we undertaken numerical computer calculations. Rather our report is intended to be a simple presentation of the important physical processes involved in nuclear cratering along with their spatial and temporal scales. We hope that this will be helpful in interpreting the results of the large scale, state-of-the-art numerical calculations and also in resolving some of the disagreements and controversies which currently exist. We recognize, of course, that the definitive theoretical work on this subject will most likely come from large computer studies which model in detail the complex phenomena involved. We recognize too that the existing database for craters formed by surface bursts of nuclear weapons is very limited and subject to a variety of interpretations. Much of what we say is probably already contained in the notebooks of workers in the field. We hope that this report will encourage a wider circulation of simple formulas and order of

magnitude calculations, so that a more complete cratering "primer" can be built up and a convergence of opinion achieved on the important mechanisms of this complex problem.

Finally, let us mention our point of view concerning the overall role of nuclear cratering. For most offensive and defensive purposes the dominant mechanism of energy coupling into the ground in surface and near surface bursts is the airblast induced ground shock, not the direct ground shock which is co-produced with the crater. The distance beyond which the relatively well understood airblast phenomena dominate the more poorly understood direct phenomena is on the order of a few crater radii. Thus, trustworthy models for crater characteristics and related phenomena are required for only a very restricted set of applications typically involving superhard or deeply buried targets. We have not studied the nature and merits of such applications but rather have accepted them as given.

1.2 Contents

We now list the contents in this report and then summarize our conclusions and recommendations. In section II we give a brief introduction to the physical phenomena which are involved in crater formation in nuclear surface bursts (i.e., radiation, hydrodynamics, elasto-plastic flow, etc.). In section III we present a discussion of scaling laws which have been applied to cratering. We begin with a review of simple dimensional analysis and then discuss some recent findings from centrifuge cratering studies. We then review the phenomenological scaling laws which have been abstracted from available data and make a few

comparisons to the centrifuge findings. Lastly we summarize comparisons between presently available computer calculations and nuclear craters formed by surface bursts.

In section IV, we present a crude calculation of the radiation coupling to the ground and the initial impulse thereby generated. This topic is a particularly critical one, since most of the energy release from modern nuclear weapons comes in the form of a short burst of kilovolt X-radiation. The controversial subject of fireball coupling is discussed here.

In section V, we discuss the hydrodynamic era in which the initial impulse produced by the radiation induced blow-off is amplified by further ejection of shock processed matter. Here, as in the preceding section, the presentation is a "back of the envelope" one aimed at order of magnitude estimates. The subsequent elasto-plastic flow is addressed in only a crude manner.

A final section (VI) presents our conclusions and recommendations. These are based in part upon the order of magnitude calculations presented in the earlier sections and in part upon the written and oral presentations we received prior to and during our studies.

This page left blank intentionally

II PHYSICAL PHENOMENA

We present here a brief discussion of the physical phenomena and regimes which are involved in nuclear crater formation. For a more detailed treatment see the reviews of Brode¹ and Knowles and Brode². The bulk of the energy release from a modern nuclear weapon is in the form of a short (~ 100 ns) burst of soft (0.5 - 2 KeV) x-rays. The remainder of the energy is in escaping neutrons, higher energy x-rays, and the internal and kinetic energies of the weapon debris, each of which may carry several percent of the total yield. Detailed code calculations are required to determine quantitatively the distribution of energy among these forms, but such is not necessary for our purposes.

The events which follow a nuclear surface burst may be divided into a series of eras, in each of which different physical processes are dominant. In the first era x-rays from the weapon stream into the ground and air, heating them to temperatures between 10^6 K and 10^7 K, lowering ("burning out") their opacity, forming a hemispherical fireball in the air, and raising the pressure in the surface layers of the ground to ~ 1000 Mbar. After the weapon has radiated most of its internal energy, in ~ 100 ns, and lost most of the remainder in adiabatic expansion, it ceases to be a source of photons although the debris kinetic energy may be significant. The heated regions of air and ground continue to expand as radiation diffuses away from the source.

On times $\gtrsim 10^{-6}$ s hydrodynamic motion becomes important, as the heated ground surface blows off into the air, sending a shock downward. Hydrodynamics replaces radiation as the mechanism of energy transport, first in the opaque ground, later in the transparent air. As the energy is distributed over more and more matter, temperatures and pressures drop and opacities rise. The ground matter, formerly fully ionized, begins to recombine. Once post-shock temperatures drop below 10^4 K and pressures below 1 Mbar, the ground is no longer ionized but only vaporized. At somewhat lower temperatures and pressures there is no vaporization. If the ground is wet then vaporization remains important for a while longer; the nuclear explosion has produced a steam explosion. But eventually even water vaporization stops and one enters the regime of nearly incompressible hydrodynamic flow.

In the era of hydrodynamic flow stresses still far exceed the yield strength of rock but are not sufficient to change significantly its volume. As the shock continues to spherically diverge and weaken, the amount of energy dissipated (its reversibility) rapidly drops. Eventually stresses drop to a few kilobars. In this regime, crucial for determining the size of the final crater, the detailed mechanical properties of the ground are important. Its strength counts, as does its behavior once it has yielded. It fractures but is not completely pulverized; the fractured material under pressure has some strength, like beach sand. Material strength and (for large craters) gravity bring the cratering process to a halt on a time scale of a few seconds. In some materials there may also be late time slumping and other adjustments of the crater shape. These too

involve the interplay between material strength and gravity and, when present, extend the cratering process to minutes or longer.

In HE (chemical) explosions temperatures are much too low for radiative exchange to be important. The cratering process begins with pressures which are characteristically 100 Kbar and temperatures of the order of a few times 10^3 K. HE cratering begins in the regime of incompressible flow and explores only the last of the eras involved in nuclear cratering. It is nevertheless of great interest since it is precisely this last era which is so sensitive to material equation of state issues and most difficult to treat theoretically. Furthermore, once the nuclear cratering process enters the incompressible flow regime it has lost all memory of what went before. Therefore one can in principle design HE experiments which reproduce all of the late time processes involved in nuclear cratering.

This page left blank intentionally

III THEORETICAL AND PHENOMENOLOGICAL SCALING LAWS

3.1 Dimensional Analysis and Centrifuge Scaling Laws

We begin by reviewing the application of dimensional analysis to the problem of cratering. This has been discussed in various degrees of completeness by many authors over the years.^{3,4} Most recently Schmidt and Holsapple⁵ have treated the subject with considerable care and thoroughness.

First consider high explosive (HE) bursts which involve the mechanical coupling of gaseous explosion products with the ground and air. We assume throughout that the ground is homogenous and unlayered. Although there has been controversy in the past, it should be obvious that the particular set of parameters chosen to describe the HE source, the ground, and the auxiliary variables have no effect on the conclusions one can draw from dimensional analysis provided one always deals with a complete set of variables. For the problem at hand we have three fundamental dimensions: length (L), mass (M) and time (T).

For definiteness we choose variables to describe the HE source as follows:

<u>Source variables</u>	<u>Symbol</u>	<u>Dimensions</u>
Total energy release (yield)	E	[ML ² /T ²]
Source specific energy	Q _e	[L ² /T ²]
Source mass density	δ	[M/L ³]

The quantities Q_e and δ are intensive variables and constant for a given type of HE; E is an extensive variable.

Since one can build from these quantities the fundamental units of L , M , and T , it follows that one can express all other variables which characterize the source as dimensionless variables π_{X1} , $\pi_{X2} \dots$ multiplied by appropriate powers of E , Q_e and δ . Some of these other source variables can be expressed trivially in terms of E , Q_e and δ [e.g., source mass $M = E/Q_e$ and source volume $V = E/(Q_e \delta)$] and hence can be ignored completely. All others are to be regarded as additional parameters which are required to completely specify the source (e.g., $\pi_{X1} = \gamma$, the specific heat ratio for the HE detonation products; $\pi_{X2} = U(Q_e)^{-1/2}$, where U is the characteristic (Chapman-Jouget) velocity of the detonation products; $\pi_{X3} =$ source aspect ratio (for non-spherical sources); etc.). Not all of these latter variables are independent. For example, if an ideal gas equation of state is assumed for the detonation products, $\pi_{X2} = (\pi_{X1} - 1)^{1/2}$. However, the equation of state of the explosive does not need to be known unless one seeks to compare cratering experiments done with different types of HE. We will assume nothing about the equation of state of the HE products.

For nuclear weapons which release energy largely in the form of radiation a more natural set of source variables might be total yield E , volume energy density $u = aT^4$, and mass M along with appropriate dimensionless variables. Since one can form fundamental variables of L , M , and T from these source variables, dimensional analysis for nuclear cratering proceeds in a manner identical to that for HE cratering.

Our choice of soil variables is the following:

<u>Soil variables</u>	<u>Symbol</u>	<u>Dimensions</u>
Mass density	ρ	[M/L ³]
Yield strength	Y	[M/LT ²]
Viscosity (kinematic)	ν	[L ² /T]

All other variables which characterize the soil, for arbitrarily complex equations of state including, for example, elastic, plastic, hysteretic, and fracture behavior, can be expressed as dimensionless variables

π_{S1} , π_{S2} , . . . times powers of the above three soil variables.

It should be emphasized that the term "viscosity" is being used here in a generic sense. It could be an actual viscosity parameter describing soil behavior, or a parameter constructed from Y , ρ and some characteristic length or time scale of the medium. For example, in an inhomogenous medium made up of grains of size ξ one can construct an effective viscosity parameter $\nu_{eff} = \xi(Y/\rho)^{1/2}$. Similarly heat conduction introduces a viscosity $\nu_{eff} = k/c\rho$ where k is the thermal conductivity and c the specific heat of the ground material. Of course, once one viscosity parameter is introduced, all others can be accounted for by dimensionless variables π_{Si} .

To illustrate the above consider the popular Coulomb-Mohr-Drucker-Prager model which is characterized by the following quantities: elastic constants K (bulk modulus), σ (Poisson's ratio), and constants C (cohesion) and ϕ (angle of internal friction) which specify the shear

value $Y = C + P \tan \phi$ at which elastic behavior fails and plastic behavior commences when the material is under hydrostatic pressure P . Also required are rules for plastic behavior and fracture. The plastic regime in this model, although complicated, is described by an equation in which strain rate is proportional to stress rate (times a non-linear function of the stresses). Such a relation describes a situation in which there is no viscosity-like parameter for the soil. Specification of fracture in the model requires an additional parameter Y_f (and perhaps one or more dimensionless parameters) as well. For brittle materials like rock the plastic regime is essentially absent; one can regard the parameters C and ϕ as specifying directly the conditions for fracture. For this latter case one could select as a complete set of soil variables: $Y = C$, $\pi_{S1} = K/C$, $\pi_{S2} = \sigma$, $\pi_{S3} = \phi$, and $v = 0$. In what follows we will not restrict our discussion by assuming any particular model of soil behavior.

In addition to the source and soil variables we must consider the following additional quantities:

<u>Auxiliary variables</u>	<u>Symbol</u>	<u>Dimension</u>
Gravity	g	$[L/T^2]$
Height (depth) of burst	h	$[L]$
Air pressure	P_a	$[M/LT^2]$
Air density	ρ_a	$[M/L^3]$
Air viscosity	μ_a	$[M/LT]$

We can form two independent, dimensionless ratios from this list

$$\pi_{A1} = \rho_a gh / P_a \quad (3.1a)$$

and

$$\pi_{A2} = \frac{\mu_a}{P_a} \sqrt{\frac{g}{h}} \quad (3.1b)$$

which we shall use in place of ρ_a and μ_a respectively. (The special case $h \rightarrow 0$ will be discussed below.) In general one has further dimensionless variables π_{A3} , π_{A4} , . . . which characterize the air medium.

Our final task is to form dimensionless ratios of soil to source variables, and auxiliary to source variables. Since we have three fundamental dimensions (M, L, and T) there are in general three independent ratios of each type. With no loss of generality we choose for the soil-source ratios:

$$\pi_{S/X1} = \frac{Y}{\delta Q_e} \quad (3.2)$$

$$\pi_{S/X2} = \frac{\rho}{\delta} \quad (3.3)$$

$$\pi_{S/X3} = \frac{v\delta^{1/3}}{E^{1/3} Q_e^{1/6}} \quad (3.4)$$

and for the auxiliary-source ratios:

$$\pi_{A/X1} = \frac{g E^{1/3}}{Q_e^{4/3} \delta^{1/3}} \quad (3.5)$$

$$\pi_{A/X2} = \frac{h(\delta Q_e)^{1/3}}{E^{1/3}} \quad (3.6)$$

$$\pi_{A/X3} = \frac{P_a}{(\delta Q_e)} \quad . \quad (3.7)$$

We are now in a position to consider any dependent variable of interest: crater volume, crater depth, peak shock at range r , etc. If we choose to consider apparent crater volume, dimensional analysis assures us that

$$V = L^3 F (\pi_{S/X}, \pi_{A/X}, \pi_X, \pi_S, \pi_A) \quad (3.8)$$

where F is some (unknown) dimensionless function of its arguments and L is any length scale in the problem. (In the above $\pi_{S/X}$ stands collectively for $\pi_{S/X1}, \pi_{S/X2}, \pi_{S/X3}; \pi_X$ for $\pi_{X1}, \pi_{X2}, \dots$; etc.) To different choices of L correspond different functions F ; all physical conclusions remain the same, however, for any choice of L . For definiteness we choose L to be the linear dimension of the HE source $L = (E/\delta Q_e)^{1/3}$ and rewrite Eq. (3.8) in the form

$$\pi_V = F(\pi_{S/X}; \pi_{A/X}; \pi_X; \pi_S; \pi_A) \quad (3.9)$$

where

$$\pi_V = \frac{V\delta Q_e}{E} .$$

Equation (3.9) expresses the dependence of crater volume on source, soil and auxiliary variables for the general case. Analogous expressions can be written down for all other dependent observables.

Now let us consider varying E for a fixed HE type, a fixed soil type and a fixed atmosphere. We ask if it is possible to vary other parameters in the problem in a manner which keeps all the arguments of F fixed. This is called a similarity transformation. By hypothesis the π_X , π_S , and π_{A3} , π_{A4} , . . . variables are unchanged and thus can be ignored. (We discuss π_{A1} and π_{A2} momentarily.) By inspection, we see that $\pi_{S/X1}$ and $\pi_{S/X2}$ are also fixed but that $\pi_{S/X3}$ which involves the soil viscosity parameter v is not fixed. We see too that $\pi_{A/X3}$ is fixed, $\pi_{A/X2}$ can be kept fixed provided we scale h according to $hE^{-1/3} = \text{const.}$, and that $\pi_{A/X1}$ will remain constant if we scale g according to $gE^{1/3} = \text{const.}$ Both of these requirements are compatible with the required constancy of π_{A1} since the latter is proportional to the product gh . However, the dimensionless air viscosity parameter π_{A2} is not invariant under these scalings.

We conclude that similar experiments are not possible even if variations of g and h are allowed whenever the soil and/or air has any significant rate dependent behavior. When soil and air viscous behaviors are absent, however, similarity is possible; for a fixed type of HE, soil, and atmosphere, one has for this special case

$$\left(\frac{V\delta Q_e}{E}\right) = F \left(\frac{Y}{\delta Q_e}, \frac{\rho}{\delta}, \pi_{S/X3} = 0; \frac{g}{Q_e} \left(\frac{E}{\delta Q_e}\right)^{1/3}, h \left(\frac{\delta Q_e}{L}\right)^{1/3}, \frac{P_a}{\delta Q_e}; \frac{\rho_a gh}{P_a}, \pi_{A2} = 0 \right) \quad (3.10)$$

where for compactness we have omitted the π_X and π_S and any additional π_A variables in the argument list of F , since they are all fixed.

Although Eq. (3.10) is general, it is inconvenient for discussing the limit $h \rightarrow 0$ since h appears twice in the argument list. It is equally general to retain only one of the h dependent variables and replace the other by the ratio of the two h dependent variables multiplied as desired by powers of one or more of the other variables in the argument list of Eq. (3.10). Hence an equivalent to Eq. (3.10) is

$$\left(\frac{V\delta Q_e}{E}\right) = F' \left(\frac{Y}{\delta Q_e}, \frac{\rho}{\delta}, \frac{g}{Q_e} \left(\frac{E}{\delta Q_e}\right)^{1/3}, h \left(\frac{\delta Q_e}{E}\right)^{1/3}, \frac{P_a}{\delta Q_e}, \frac{\rho_a}{\rho} \right) . \quad (3.10')$$

3.1.1 Zero Height of Burst

If we continue to discuss the case where viscosities play no important role and specialize to zero height of burst then Eq. (3.10') implies

$$\left(\frac{V\delta Q_e}{E}\right) = G \left(\frac{Y}{\delta Q_e}, \frac{\rho}{\delta}, \frac{g}{Q_e} \left(\frac{E}{\delta Q_e}\right)^{1/3}, \frac{P_a}{\delta Q_w}, \frac{\rho_a}{\delta} \right) \quad (3.11)$$

or equivalently

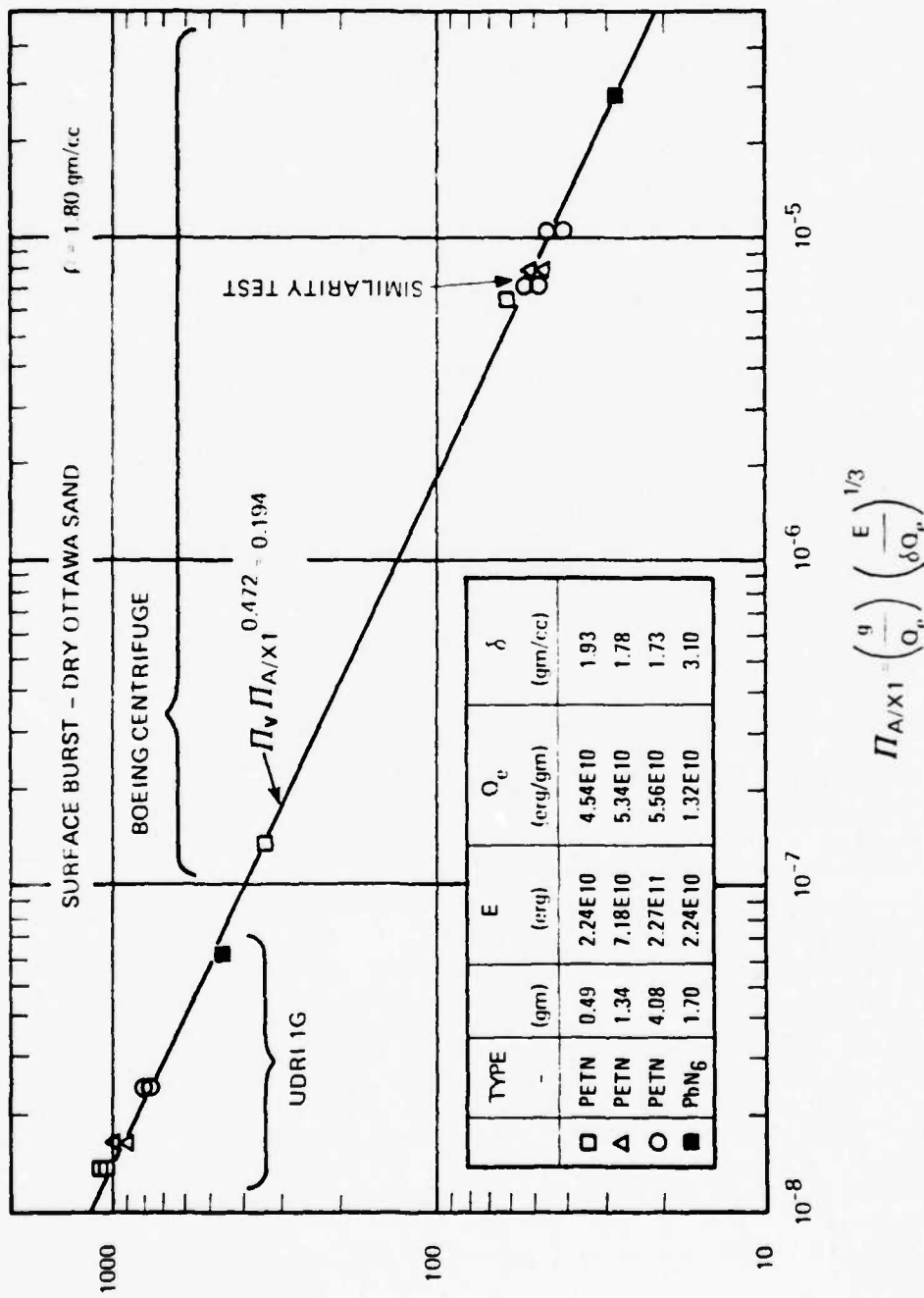
$$\pi_V = G(\pi_{S/X1}, \pi_{S/X2}, \pi_{A/X1}, \pi_{A/X3}, \pi') \quad (3.11')$$

where G stands for F' with its fourth argument set to zero and

$\pi' = \frac{\rho_a}{\delta} = \frac{\pi_{A1} + \pi_{A/X3}}{\pi_{A/X2} + \pi_{A/X1}}$ has been introduced for convenience. Certain

features of Eq. (3.11) can be tested by doing experiments in accelerated reference frames, centrifuges being the most convenient. Note that for fixed soil, air and HE type the only independent variable is the combination $gE^{1/3}$. Thus either g or E or both may be varied to determine the functional form of G .

To our knowledge the only relevant centrifuge experiments which have been carried out to date are those of Schmidt and Holsapple at Boeing.^{5,6} These complement the work done at normal gravity by Piekutowski⁷ at the University of Dayton Research Institute. The early Boeing work was done in dry Ottawa sand, a material which has little or no cohesion ($\gamma \approx 0$) and is expected to have little or no rate dependent effects ($v \approx 0$). Some results are shown in Fig. 3.1. The points labeled "Similarity Test" correspond to two shots at different g values with yields differing by a factor of 3 but having a common value of $gE^{1/3}$. The expected similarity is confirmed and the reproducibility of the results demonstrated as well. (Actually as indicated on the figure the effective values of δ and Q_e for the two cases differ slightly because of the



$$\left(\frac{\varepsilon}{\delta \Omega_e} \right) = V_U$$

$$\Pi_A/x_1 \left(\frac{q}{\Omega_e} \right) \left(\frac{\varepsilon}{\delta \Omega_e} \right)^{1/3}$$

Figure 3.1 CRATER VOLUMES VS GRAVITY STRENGTH FOR ZERO HEIGHT OF BURST HE SHOTS OVER OTTAWA SAND. NOTE THE HIGH REPRODUCIBILITY OF THE CRATER VOLUMES UNDER THESE WELL CONTROLLED LABORATORY SITUATIONS. (Source: ref. 5)

presence of the initiator which constitutes a nontrivial fraction of the explosive for these rather small shots. In recognition of this, the authors of ref. 5 have chosen to adjust by selecting g to keep $\tau_{A/X1} = (g/Q_e)(E/\delta Q_e)^{1/3}$ constant rather than simply $gE^{1/3}$. Also shown in Fig. 3.1 is a third shot at a nearby value of $\tau_{A/X1}$ which gives a nearby value for scaled crater volume thus indicating similarity over an 8.3:1 range of E . While this is not an extensive range of E it does give strong experimental support to the notion of centrifuge scaling. Taken seriously these shots, done with a few grams of explosive at $g \approx (300 - 460) g_0$, are equivalent to TNT yields at normal gravity ($E \propto g^3$) of $E = 6 \times 10^{18}$ ergs = 0.14 KT (g_0 = terrestrial value of gravity).

It is interesting, too, that dry sand, although not expected to display actual viscous behavior, does have a characteristic length scale set by grain size which as described above can act as an effective viscosity. The authors of ref. 5 report that crater sizes at the g values used in their work seem to be insensitive to grain size.

There is also another hidden "size" parameter in the centrifuge work. Since the sample size is finite in depth and radius it is possible that reflections from the walls or bottom of the sample container influence the final crater size or shape. It is easy to test for the presence of such effects by varying sample sizes, by putting absorbing material on the sample boundaries, etc. One can also test experimentally for other unwanted influences such as Coriolis effects and surface winds. Schmidt

and Holsapple report that there is no sign that these latter influences are present in their work thus far, particularly for dry granular material.

Dimensional analysis says nothing about the functional dependence of G upon its arguments, in particular upon $\pi_{A/X1}$. By making additional assumptions, some simplified cases can be examined. If we consider the limit of a cohesionless material $Y/(\delta Q_e) \rightarrow 0$, negligible atmospheric effects $P_a/\delta Q_e \rightarrow 0$, $\rho_a/\delta \rightarrow 0$, and assume that the crater volume V is independent of the source specific energy density Q_e , it follows that G must be of the form

$$G(0, \frac{\rho}{\delta}, \pi_{A/X1}, 0, 0) = (\pi_{A/X1})^{-\alpha} f\left(\frac{\rho}{\delta}\right) = \left(\frac{gE^{1/3}}{Q_e^{4/3} \delta^{1/3}}\right)^{-\alpha} g f\left(\frac{\rho}{\delta}\right) \quad (3.12)$$

where $\alpha_g = 3/4$ since Q_e appears linearly on the left hand side of Eq. (3.11). Here f is an unknown function of its argument but is constant for fixed HE and soil combinations. Hence for this special case,

$$V = \text{const } \left(\frac{E}{g\delta}\right)^{3/4}, \quad (3.13)$$

a result often referred to as gravity scaling.

One can ask if Eq. (3.12), or equivalently (3.13), is satisfied by HE bursts. The answer for Ottawa sand is negative as shown in Fig. 3.1. Remarkably the functional dependence of G for this material over a wide range is, however, well fitted by the simple form

$$\pi_V = \text{const } (\pi_{A/X_1})^\alpha , \quad (3.14)$$

where the experimental value of the exponent is $\alpha = 0.472 \pm 0.010$, clearly different from $\alpha_g = 3/4$. This difference means that the crater volume for this material depends not only on the total energy release E but also on the specific energy Q_e . This was also directly demonstrated by comparison of lead azide and PETN shots. An equivalent statement is that V depends on E and the source volume $V_X = (E/\delta Q_e)$, i.e., the crater "remembers" the size of the explosive. This violates no general principles but shows that the key assumption behind the gravity scaling argument is incorrect for values of Q_e in the range $(1-5 \times 10^{10}$ ergs/gm) used in the experiments. The dependence or independence of V on Q_e in other ranges is an open question but clearly an important one, when one contemplates extrapolation to nuclear energy densities. Hypervelocity impact cratering is therefore of great interest since it extends Q_e to values well above the range accessible with chemical explosives. In detailed experiments, Schmidt and Holsapple have observed that the Q_e dependence expressed by Eq. (3.14) holds also for impact velocities from 0.5 km/s to 7 km/s which corresponds to a 200:1 ratio for Q_e and a maximum Q_e of 2×10^{11} ergs/gm.

A second special case is the limit in which gravity effects are negligible compared to material strength effects. In this case the dimensionless variable π_{A/X_1} drops out of the problem and Eq. (3.11) reduces to

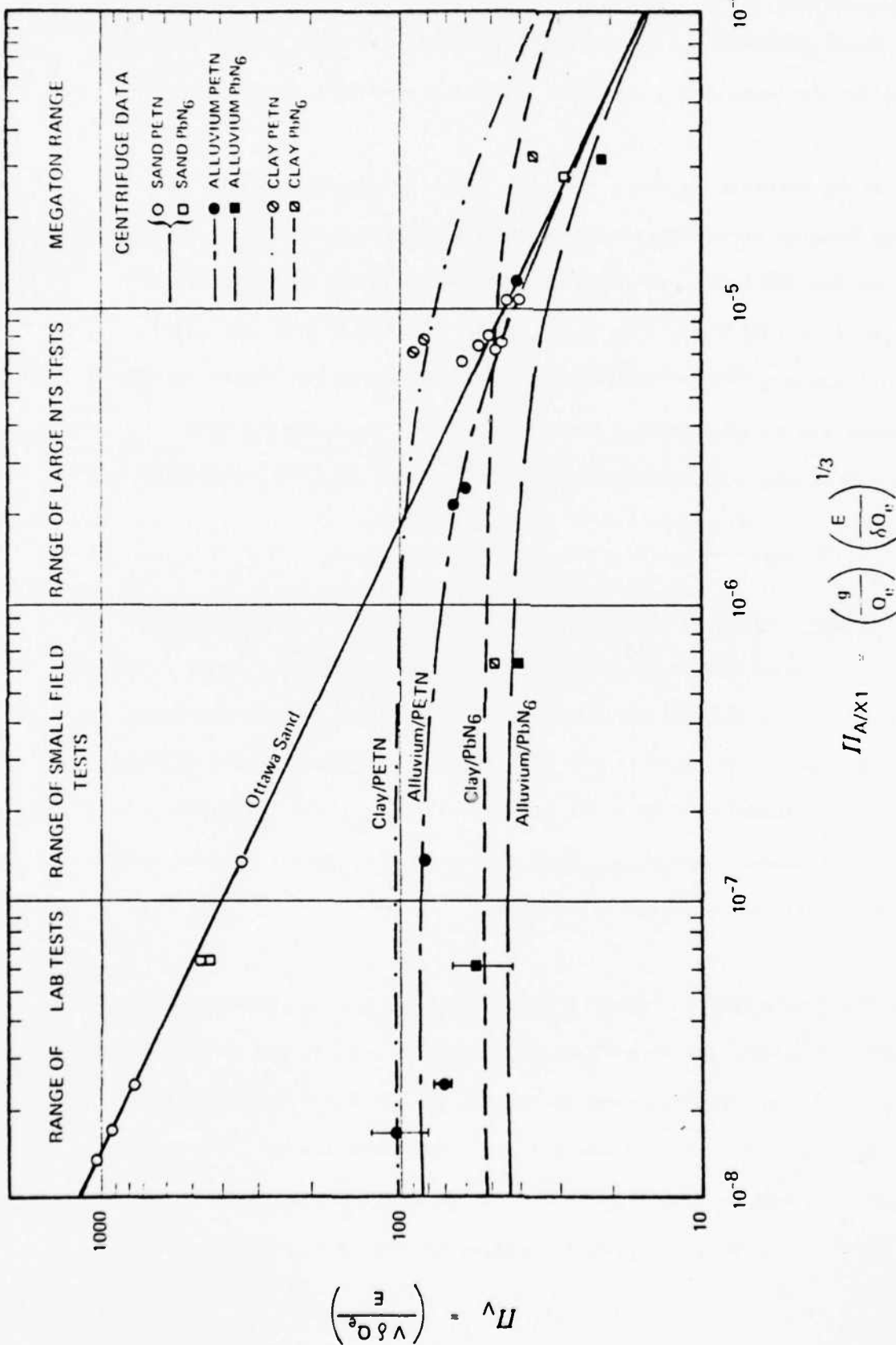
$$V = E \left(\frac{1}{\delta Q_e} \right) G \left(\frac{Y}{\delta Q_e}, \frac{\rho}{\delta}, 0, \frac{P_a}{\delta Q_e}, \frac{\rho_a}{\delta} \right) \quad (3.15)$$

This is the familiar "cube root" scaling law. Although this law is often assumed in crater scaling phenomenology it has no fundamental basis. In contrast, for air bursts it is physically plausible that gravity plays an insignificant role; indeed, cube root scaling is observed as predicted.⁸ Note that even when it applies, Eq. (3.15) says nothing about the dependence of crater volume on material properties. To determine this one must do actual or numerical experiments.

Centrifuge experiments⁶ in Kirtland Air Force Base (KAFB) alluvium exhibit an approximate cube root regime as shown in Fig. 3.2 and also a nontrivial dependence on explosive type. Fig. 3.2 also shows that at high g values crater volumes in alluvium and clay no longer grow linearly with energy release. Holsapple and Schmidt⁶ have been able to find a simple parametrization of all of their data in terms of two (Coulomb-Mohr) material parameters: cohesion and angle of internal friction

$$V = \left(\frac{E}{\delta Q_e} \right) (0.174) \left[\frac{C}{\rho Q_e} + \frac{g}{Q_e} \left(\frac{E}{\delta Q_e} \right)^{1/3} \{ \tan \phi + 0.1 \} \right]^{-0.472} \quad (3.16)$$

Curves corresponding to this formula are shown on Fig. 3.2 and represent well the general features of the data. Centrifuge results for wet sands⁹



III-15

Figure 3.2. CRATER VOLUMES AT ZERO HEIGHT OF BURST AS A FUNCTION OF GRAVITY SCALED YIELD FOR VARIOUS SOILS. THE CURVES CORRESPOND TO THE FORMULA DEVELOPED IN REF. 6 AND REPRODUCED AS EO. (3.16) OF THIS REPORT. THE RANGES INDICATED AT THE TOP OF THE FIGURE CORRESPOND TO NORMAL GRAVITY. (Source: ref. 6)

are also describable by Eq. (3.16) using an effective value of ϕ less than that for dry sand and a non-zero effective cohesion parameter C .

It is interesting, too, that the above formula based only on centrifuge studies correctly predicts the apparent crater volumes obtained in alluvium for TNT bursts of 5000 and 256 lbs done in the field at the Nevada Test Site (NTS)--see Fig. 3.3. (Note that these data are only barely into the gravity-influenced regime. The correction factor to cube root scaling due to the gravity term in Eq. (3.16) corresponds to a reduction in apparent crater volume of only 11% and 25% for the lighter and heavier shots respectively.)

Although the form of Eq. (3.16) can be partially motivated by energy balance considerations, it must in the end be regarded as a phenomenological expression which may require modification for materials more complex than those used in its development. It does, however, stand as an important reminder that there can be various regimes (cohesion dominated, gravity influenced, gravity dominated, etc.) in cratering which render naive extrapolations meaningless.

The dependence of crater radius r and depth d on material properties and source variables has also been explored in the centrifuge crater work.¹⁰ The patterns seen in the radius and depth variables are somewhat more complicated than those described by the volume formula, Eq. (3.16). As explosive yield moves from the cohesion dominated regime (small E at g_0) into the gravity influenced regime (larger E at g_0)

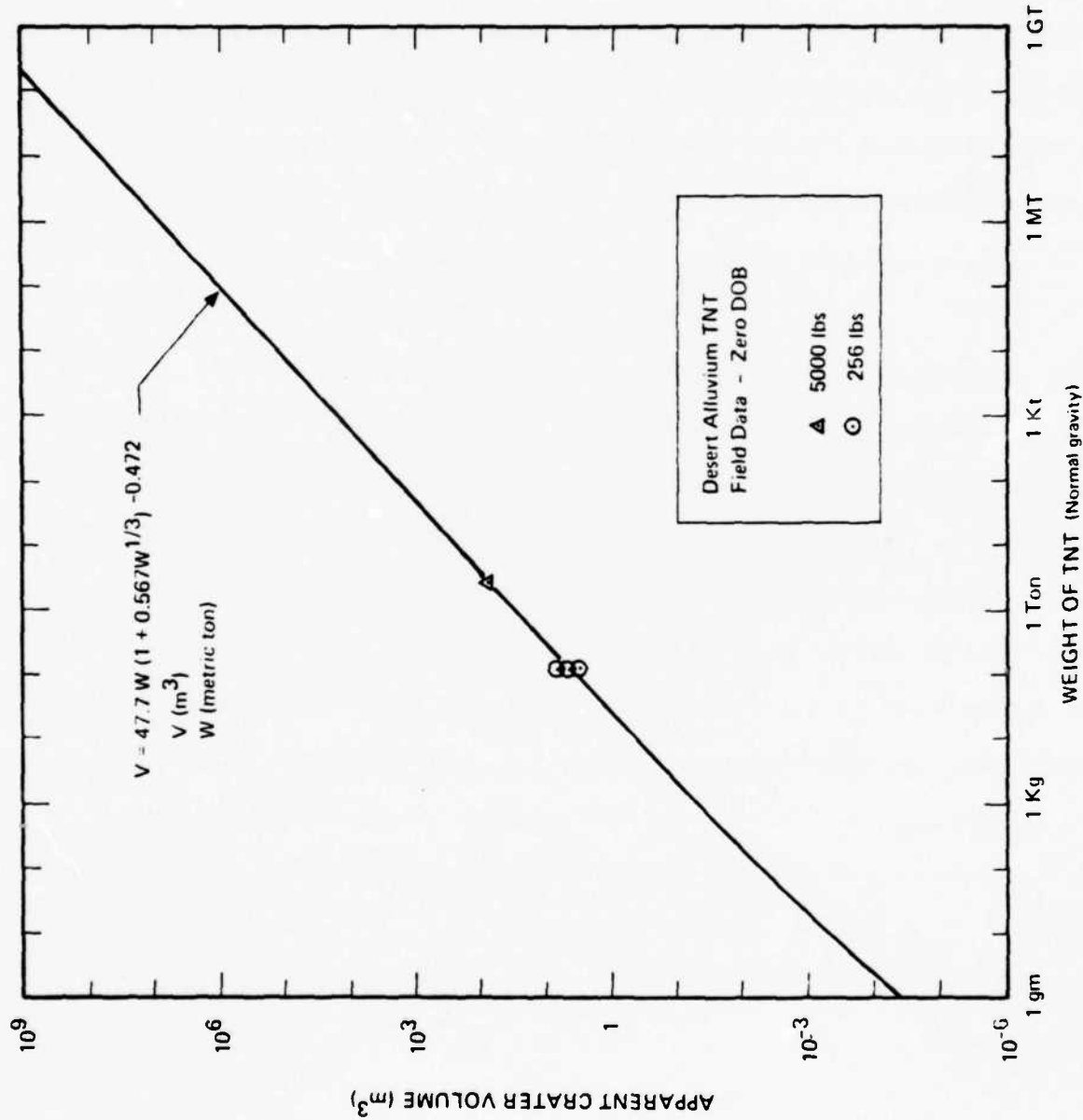


Figure 3.3 CRATER VOLUME VS YIELD (EQUIVALENTLY MASS) FOR TNT AT ZERO HEIGHT OF BURST OVER ALLUVIUM. THE CURVE CORRESPONDS TO EQ. (3.16) WITH PARAMETERS DETERMINED ENTIRELY BY CENTRIFUGE CRATER STUDIES. (Source: ref. 6)

the crater aspect ratio r/d increases suggesting that stability considerations are becoming important. The same trend of increasing aspect ratio with increasing crater size is well known in the PPG nuclear crater results (see Fig. 3.4) and also in earth impact crater observations. Of course in these latter two cases geological layering and other phenomena may also be playing a role. Nevertheless, the trend of the centrifuge results are notable and would seem to indicate that phenomena important to large scale craters are being probed by the centrifuge studies.

3.1.2 Non-Zero Heights of Burst

All of the above centrifuge crater results were for zero height of burst which by definition correspond to a half buried spherical charge distribution. Only very limited results are presently available for non-zero h values. Most are for tangent above charge emplacements, i.e., $h = +a$ (charge radius) over Ottawa sand. Preliminary results¹¹ indicate that for this cohesionless material crater volume departs even more strongly from cube root scaling for positive h than the fit to the $h = 0$ data described by Eq. (3.14). There seems to be an additional dependence of π_V on source specific energy beyond that included in the dimensionless variables π_{A/X_1} (gravity scaled yield) and π_{A/X_2} (scaled height). This could indicate that the scaled atmospheric pressure variable π_{A/X_3} is playing a role.

For negative values of h Schmidt and Holsapple report¹¹ that two tangent-below ($h = -a$) shots of the same HE type in Ottawa sand at different g and E values, but common $gE^{1/3}$, show similarity as was

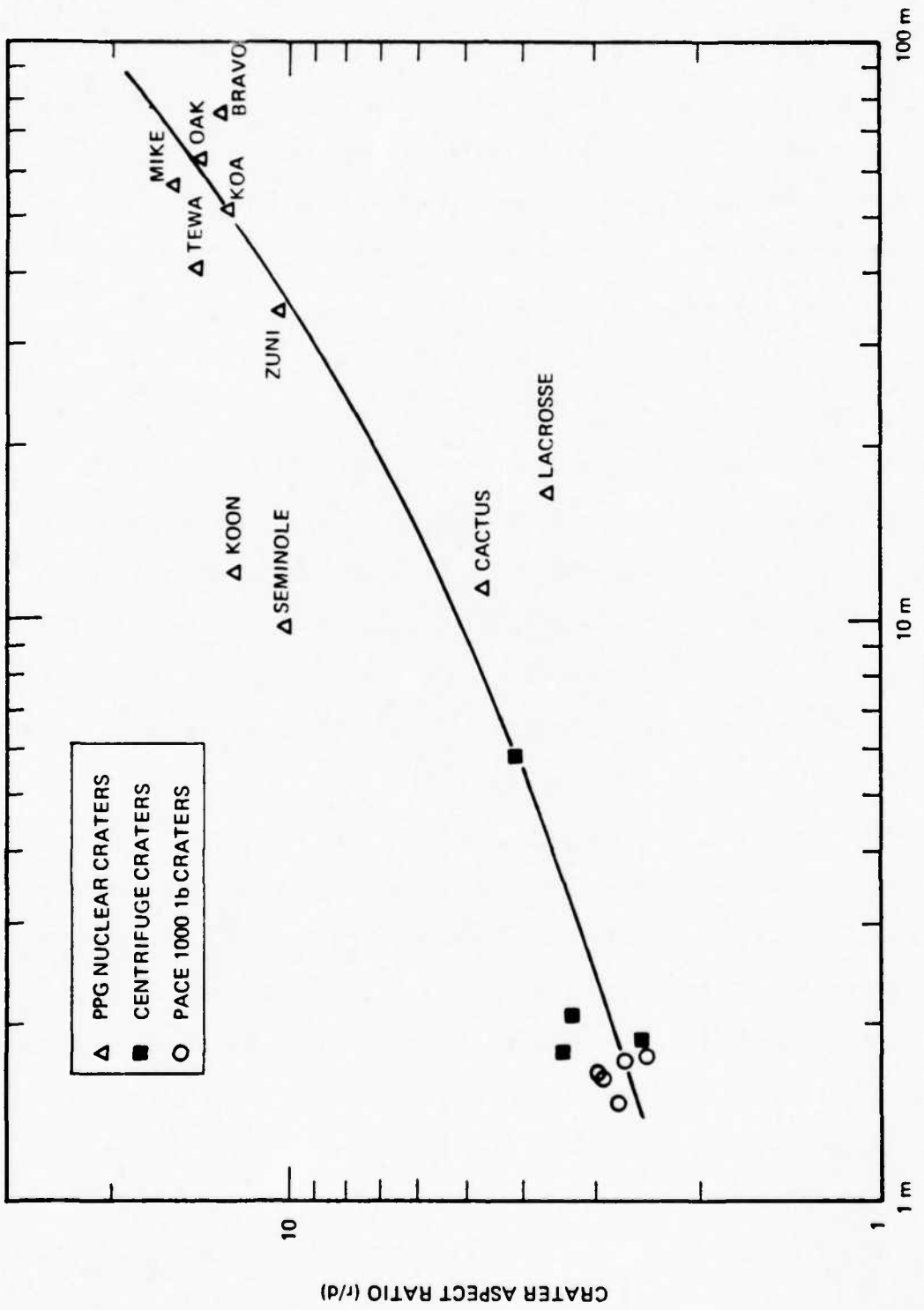


Figure 3.4 THE TREND OF CRATER ASPECT RATIO R/D WITH CRATER DEPTH D FOR SURFACE AND NEAR SURFACE BURSTS FOR NUCLEAR AND HE SOURCES AT NORMAL GRAVITY AND HE CRATERS AT ENHANCED GRAVITY. THE CENTRIFUGE CRATER DEPTHS HAVE BEEN SCALED BY g AS REQUIRED BY SIMILARITY. THE CENTRIFUGE CRATERING MEDIUM WAS WET SAND. (Source: ref. 9)

observed at $h = 0$. These workers have also achieved⁹ successful centrifuge simulations in alluvium of the 20 T Stagecoach III ($h = -3.77$ a) and 20 T Jangle HE 2 ($h = -1.19$ a) TNT shots. These complement the successful ($\pm 20\%$) simulation¹² of the shallow buried 0.5 KT nuclear Johnie Boy event ($h = -0.64$ a) done early in the centrifuge program. The centrifuge HE charge equivalent for Johnie Boy was established by applying the centrifuge scaling law $gE^{1/3} = \text{const.}$ to the full scale HE equivalent charge calculated in ref. (13).

3.2 Phenomenological Scaling Laws

It has not been possible to obtain scaling laws for near-surface burst cratering by a direct study of the underlying equations of motion and equations of state. This contrasts with the rather well understood situation for the blast wave produced by atmospheric bursts. Consequently a great deal of work has been devoted to the development of phenomenological scaling laws based on field data. Many HE cratering experiments have been done to further these efforts. A recent and comprehensive scaling phenomenology is that developed by Cooper¹⁴ and coworkers¹⁵; it forms the basis of the prediction curves given in the Air Force Manual for Design and Analysis of Hardened Structures¹⁶ and in the DNA Effects Manual.¹⁷ Alternative phenomenologies exist as well, e.g., Refs. (3), (4) and (17a). The latter approach^{17a} due to Lilley challenges the notion that nuclear sources must be separated into low energy density and high energy density categories as done by Cooper, et al.

Strong assumptions must be made concerning the form of the phenomenological scaling laws in order to make any progress. There do not

exist sufficient data to fully test these assumptions. The primary assumption of Cooper is that the apparent crater volume V is given by the product of three factors: yield E (cube root scaling), a constant η which contains all the effects due to material properties and geology, and ϕ_i , a function which depends on the scaled depth of burst D and weapon type i [$i = \text{HE}$, NE (non-radiating), NE (radiating)]. Namely

$$V = E\eta\phi_i(D) . \quad (3.17)$$

With no loss of generality we can take $\phi_{\text{HE}}(0) = 1$. Then by virtue of the assumed form of Eq. (3.17), the values of $\phi_{\text{NE}}^{\text{rad}}(0)$ and $\phi_{\text{NE}}^{\text{non-rad}}(0)$ give the so-called relative efficiencies for cratering by radiating and non-radiating nuclear bursts, respectively, in any geology. Similarly the ratio $r_{\alpha/\beta} \equiv \eta(\alpha)/\eta(\beta)$ gives the relative cratering efficiency in geology α to that in geology β for any type source assuming the validity of Eq. (3.17).

Central to Cooper's approach is the further assumption that all dependent and independent lengths are to be scaled by $V^{1/3}$. In particular in Eq. (3.17)

$$D = d/V^{1/3} \quad (3.18)$$

where d is the actual depth of burst. (Note d here corresponds to $-h$ used in subsection 3.1 above.) As a consequence of this scaling rule the dependent variable V appears on both sides of Eq. (3.17). However, by rewriting Eq. (3.17) in the form

$$\frac{V}{\eta E} = \phi_i \left(\frac{d}{(\eta E)^{1/3}} \left(\frac{\eta E}{V} \right)^{1/3} \right) \quad (3.19)$$

and solving for $\frac{V}{\eta E}$ we can re-express it in the form

$$V = \eta E \psi_i \left(\frac{d}{(\eta E)^{1/3}} \right) \quad (3.20)$$

This is a canonical cube root scaling law in terms of an "effective" yield ηE . Note that the height (depth) of burst function ψ_i depends on source type i but is independent of material properties; all dependence on the latter has been swept into an effective yield variable.

Equation (3.20), or equivalently (3.17), implies strong statements about the crater volume. In particular the cube root dependence allows no dependence on gravity for even the largest craters. Evidence for such a cube root scaling law for HE surface bursts seems to be based mostly on field tests done with 256 and 1000 lb TNT charges in cohesive soils (alluvium tuff, playa, clays, wet sands, etc.). Reproducibility in a given geology shows scatter of a factor of 2 to 3 due presumably to site inhomogeneities and variations.¹⁸ These variations can mask small but real effects which might be important for extrapolations to yields in the kiloton and higher ranges. Indeed, the centrifuge cratering experiments mentioned earlier, when scaled to normal gravity predict that departures from cube root scaling will show up in precisely this yield range, e.g., they indicate a factor of 2 effect in alluvium at $E \approx 1$ KT and zero height of burst. (See Fig. 3.4).

Cooper's fit to the $\phi_{HE}(D)$ for $-0.8 < D < 0.8$ is shown in Fig. 3.5 along with η values (cratering efficiency) for generic geologies. Note there is considerable spread in the data about the best fit line.

Next consider near surface nuclear cratering. Here the database (See Table I) is extremely limited and field conditions poorly documented. In the unclassified literature, there exist data for two low yield, low energy density shots done over alluvium at the NTS and ten high yield shots over coral at the PPG. Of these latter, two (KOA and SEMINOLE) were done in water tanks and hence are usually considered to be equivalent to low energy density nuclear shots. The remaining eight PPG bursts are thought to resemble modern high energy density weapons for which most of the energy release occurs as X radiation. However, as has been emphasized by many authors, it is not clear that any of these weapons coupled a significant amount of energy to the ground directly by radiation since the weapons were surrounded by experimental equipment and sheds and in some cases were detonated on barges.

Because of the limitations of the nuclear database one has little chance of testing the cube root scaling assumption and the $V^{1/3}$ rule for scaling the height of burst. All one can do is make these assumptions and then use the data to find the height of burst curve $\phi_{NE}(D)$. The results are shown in Fig. 3.6. In the Cooper model two separate curves are necessary, one for low energy density sources, $\phi_{NE}^{\text{non-rad}}$, and one for high energy density, ϕ_{NE}^{rad} . For the reasons stated above, KOA and SEMINOLE have been combined with the NTS alluvium shots using the results from small

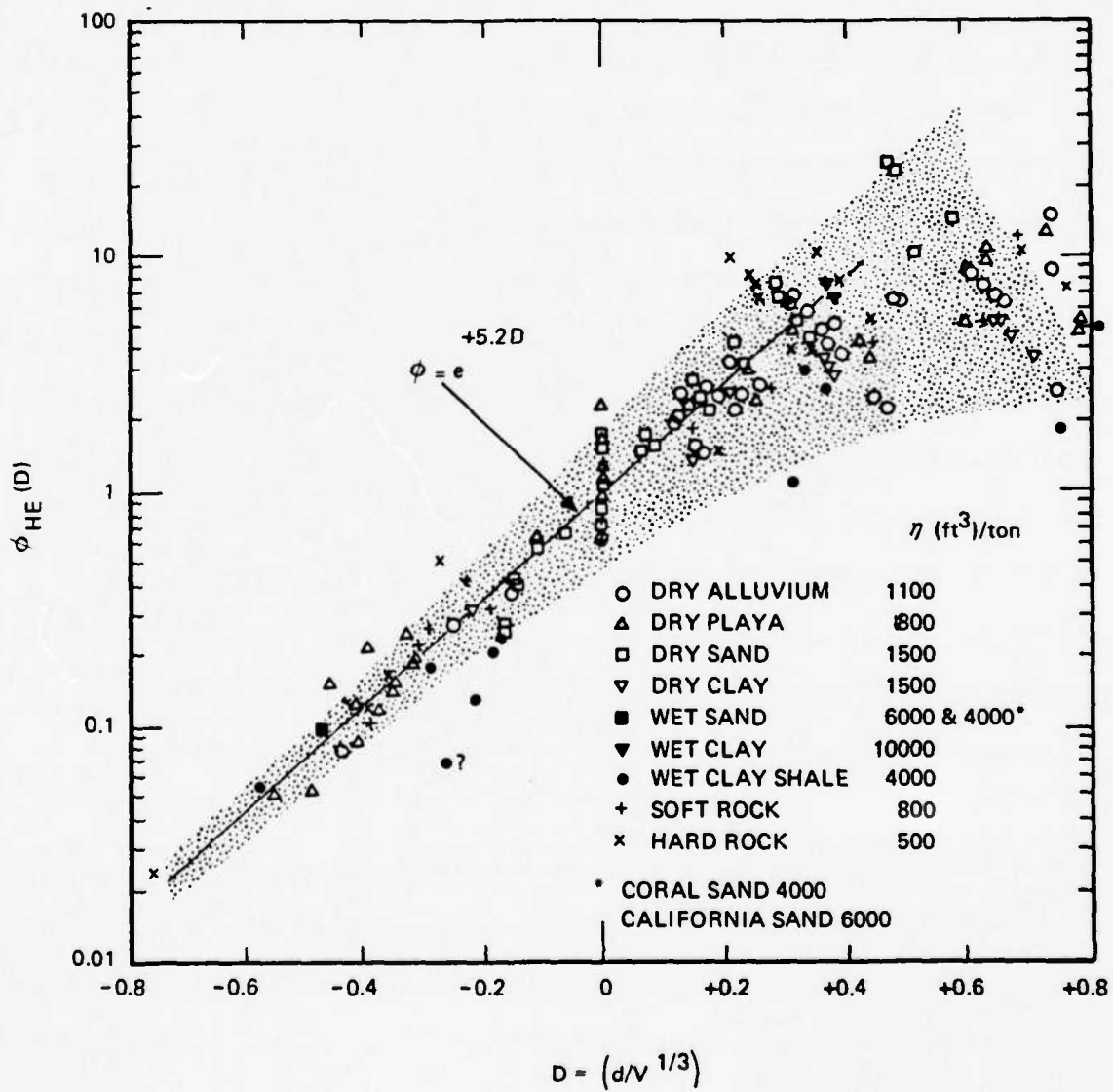
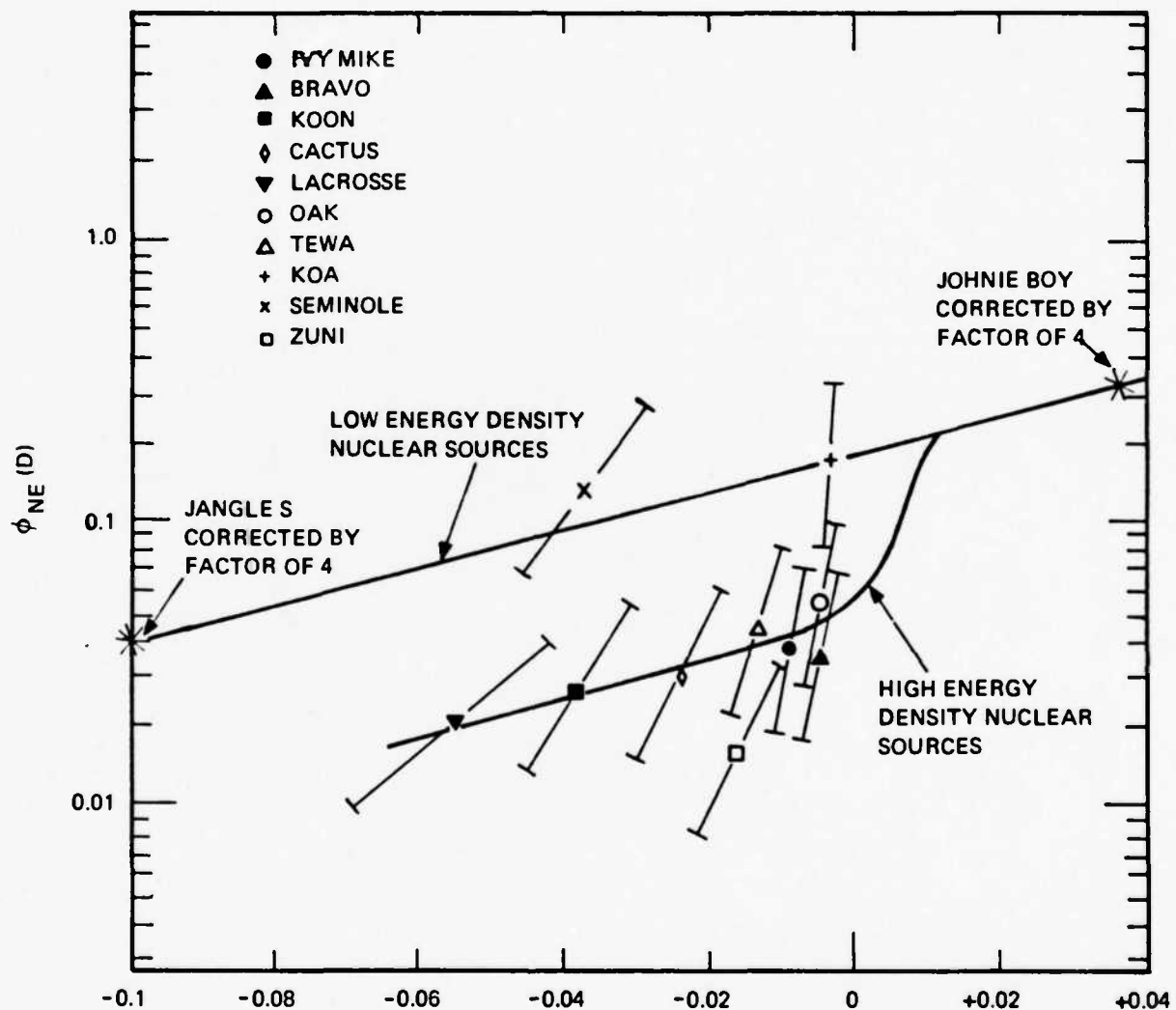


Figure 3.5 THE HEIGHT OF BURST CURVE FOR HE (ALL GEOLOGIES) NORMALIZED ACCORDING TO $\phi_{HE}(0) = 1$. ALSO SHOWN ARE VALUES OF THE "HE CRATERING EFFICIENCY" η FOR GENERIC SOURCES. (Source: ref. 14)

TABLE I
CRATER PARAMETERS FOR NUCLEAR SURFACE BURSTS

EVENT	YIELD	HOB (ft)	MEDIUM	RADIUS(r) (ft)	DEPTH(d) (ft)	VOLUME(V) (ft ³)	V/E (ft ³ /ton)	HOB/V ^{1/3}	r/V ^{1/3}	d/V ^{1/3}
<u>Non-radiating (low energy density)</u>										
JANGLE S										
JANGLE S	1.2 KT	+3.5	NTS Alluvium	45	1.7	4.45 × 10 ⁴	37	+0.099	1.27	0.48
JOHNNIE BOY	0.5 KT	-1.75	"	61	30	1.4 × 10 ⁵	280	-0.034	1.17	0.578
KOA (water tank)	1.3 MT	3	PPG Coral Sand	2310	171	8.11 × 10 ⁸	624	0.0032	2.48	0.183
SEMINOLE (water tank)	13.7 KT	7	"	324	32.2	6.99 × 10 ⁶	510	0.037	1.69	0.168
<u>Radiating (high energy density)</u>										
ZUNI	3.4 MT	9.6	PPG Coral Sand	1145	113	2.04 × 10 ⁸	60	0.010	1.94	0.192
TEWA	4.6 MT	12.3	"	2160	129	7.63 × 10 ⁸	164	0.013	2.36	0.141
LACROSSE	39.5 KT	8	"	200	46.5	3.06 × 10 ⁶	77	0.055	1.38	0.32
IVY MIKE	10.4 MT	10	"	3275	187	1.44 × 10 ⁹	138	0.0089	2.9	0.166
CASTLE BRAVO	15 MT	7	"	3180	225	2.01 × 10 ⁹	134	0.0055	2.52	0.178
CASTLE KOON	150 KT	9.3	"	538	75	1.5 × 10 ⁷	100	0.038	2.18	0.304
CACTUS	18 KT	3	"	173	37.2	1.99 × 10 ⁶	111	0.024	1.38	0.0296
OAK	9 MT	6.5	"	3200	203	1.83 × 10 ⁹	203	0.0053	2.62	0.166



$$D = \left(\frac{d}{V} \right)^{1/3}$$

Figure 3.6 THE HEIGHT OF BURST CURVES FOR RADIATING (HIGH ENERGY DENSITY) AND NON-RADIATING (LOW ENERGY DENSITY) NUCLEAR SOURCES. THE VALUES OF THESE CURVES AT $D=0$ GIVE THE RELATIVE CRATERING EFFICIENCIES FOR THESE SOURCES VS HE SOURCES. THE PRODUCT OF $\Phi_{NE}(0)$ AND THE η VALUE FROM FIG. 3.5 GIVES THE NE CRATERING EFFICIENCY ACCORDING TO THE PHENOMENOLOGY BEING DESCRIBED. (Adapted from ref. 14)

HE cratering shots $n_{\text{coral}}/n_{\text{alluvium}} = 4$. Since the two NTS and these two PPG craters have very different aspect ratios, it is not clear whether this manner of comparison has any meaning. The manner in which the $\phi_{\text{NE}}^{\text{rad}}$ and $\phi_{\text{HE}}^{\text{non-rad}}$ curves merge at large positive and negative values of D is a matter of speculation and is at present unconstrained by experiment.

Note that when treated in the above manner the dependence of crater volume, and presumably other observables, is a very steep function of height/depth of burst in the neighborhood of $D = 0$. This is very unfortunate since one is interested in precisely this near-surface burst regime. The extreme weakness of any phenomenology based on the PPG craters is underlined by the progressive flattening of the craters (increase in aspect ratio) with yield value, a feature not observed in either the HE or NE craters at the NTS nor the 1000 lb HE craters at the PPG--see Fig. 3.7.

The very thorough and extensive restudy of the PPG craters by Ristvet et al.¹⁹ has concluded that for at least MIKE, KOA and OAK much of the apparent crater volume resulted from compaction of the underlying coral medium along with shape changes due to liquification and late time gravity slumping. Extrapolation of PPG data to other geologies by simple methods may therefore have no meaning whatsoever.

The phenomenology of Cooper and coworkers goes beyond prediction for apparent crater volume to cover such observables as crater radius, crater depth, peak shock at range r , etc. In all of these the $v^{1/3}$ length scaling rule is adopted. Since in all of these cases one is scaling

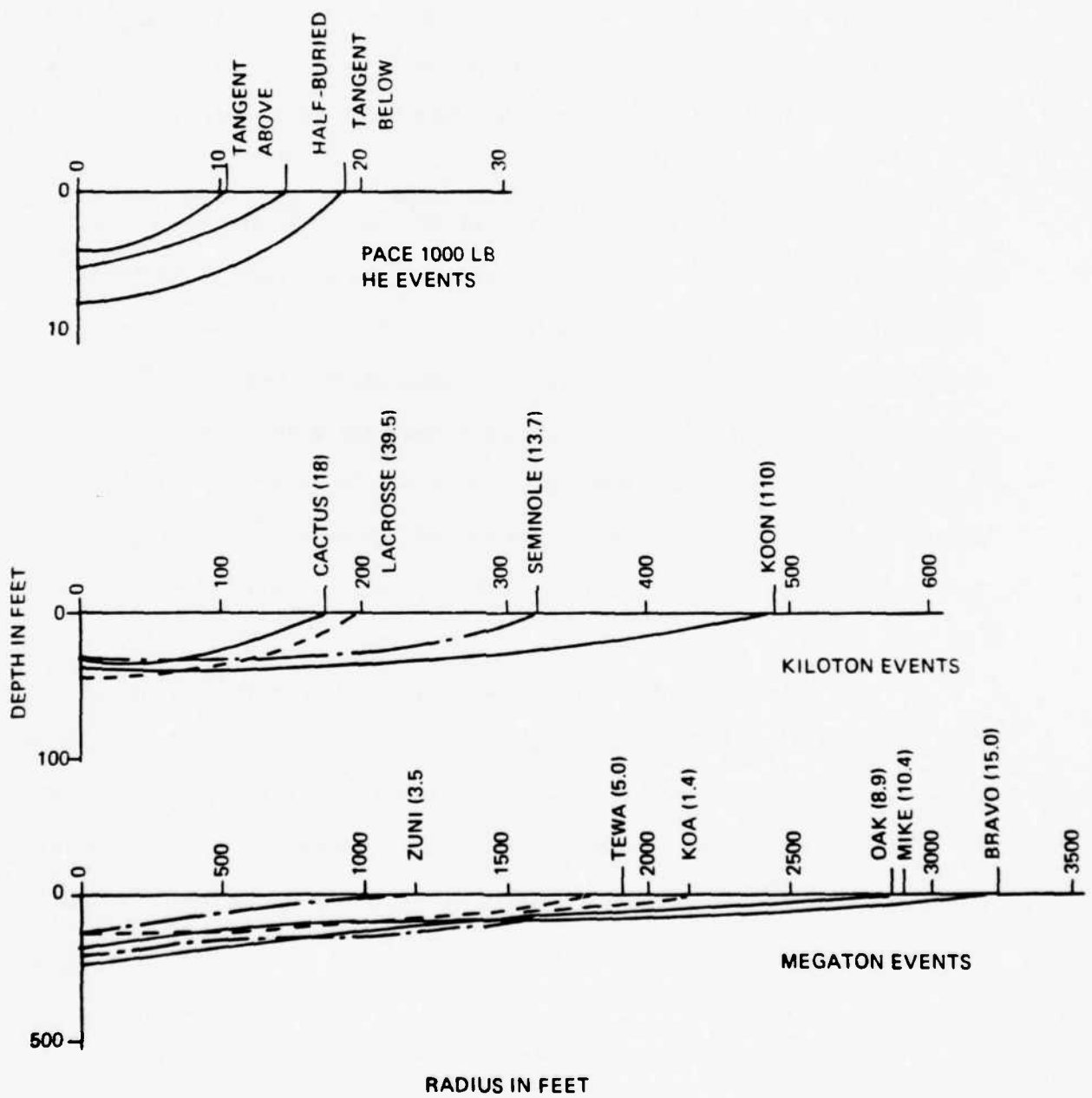


Figure 3.7 AVERAGED CROSS SECTIONS THROUGH HE AND HE CRATERS FORMED IN PPG CORAL. NOTE THE PROGRESSIVE FLATTENING (INCREASE IN ASPECT RATIO) AS CRATER SIZE INCREASES. (Source: ref. 19)

a dependent variable by another dependent variable, (crater volume), there is some reason to hope that even if the assumptions behind Eq. (3.17) for V are not fully correct for nuclear and HE bursts in the KT-MT range, the predictions for other effects may nevertheless have some validity. Centrifuge studies could shed light on $v^{1/3}$ scaling. Insufficient data are presently available.

3.3 Comparison Between Theory and Experiment

There exists no case for which a computer code calculation has been carried all the way to cratering in a geology and configuration appropriate to a PPG radiating nuclear burst. Consequently all comparisons between code results and the PPG database make use of the scaling phenomenology discussed in the last subsection, or some other phenomenology, and are therefore correspondingly uncertain. For non-radiating nuclear bursts two code calculations exist which go all the way to late state crater formation: (i) a calculation²⁰ for KOA, a 1.3 MT burst exploded in a water tank at the PPG and (ii) a calculation²¹ for JOHNIE BOY, a 0.5 KT explosion buried in NTS alluvium at a depth of 0.585 m.

For HE bursts the situation is somewhat better although the number of cases in which one can make actual comparisons of code results and field data is still quite limited. Accurate characterization of field geology and material properties has proven to be quite complex at even the best of sites. The best documented HE crater calculations seem to be: (i) MIXED COMPANY - III (0.5 KT), a tangent-above burst on siltstone/ sandstone²²; (ii) MIDDLE GUST - I (0.02 KT), half buried in layered clay/shale²³; and

(iii) MIDDLE GUST - III, and - IV (0.1 KT), tangent-above over layered clay/shale.²³

Comparisons between code predictions and experiment for non-radiating nuclear and HE are shown in Tables II and III respectively. One notes that the situation is in reasonably good shape for the HE case. There is even good agreement in some cases between code predictions for the ground shock patterns and observations provided material parameters appropriate to the in situ case are used. This agreement has only been achieved after considerable post shot refinement of the computer models, however.

For the low energy density nuclear case the situation is mixed. For the one small yield NTS burst the agreement in all crater parameters is quite satisfactory but for the large yield PPG burst the predicted crater aspect ratio is in disagreement with the observed value even though the volume is comparable. Details of the KOA code calculation²⁰ are unknown to us at the present time. In particular we do not know if the coral compaction which contributes to much of KOA crater volume, as indicated by the resurvey¹⁹, was modeled in the code calculations. Nor do we know if liquification and gravity slumping (mechanisms often mentioned as responsible for the high aspect ratios of the PPG craters) were permitted by the code.

As mentioned already, no direct tests of the code calculations for crater formation by radiating nuclear weapons are available. In Table IV

COMPARISON OF CRATER DIMENSIONS;

Non-Radiating Nuclear. Code Predictions in ().

TABLE II

<u>EVENT</u>	<u>YIELD (KT)</u>	<u>RADIUS (ft)</u>	<u>DEPTH (ft)</u>	<u>VOLUME (ft³)</u>
JOHNIE BOY (Shallow Buried)	0.50	72 (69)	40 (46)	2.1×10^5 (3.4×10^5)
KOA (Water Tank)	1.3×10^3	2,310 (70)	171 (450)	8.1×10^8 (5.3×10^8)

TABLE III
COMPARISON OF CRATER DIMENSIONS;
High Explosive. Code Predictions in ().

<u>EVENT</u>	<u>YIELD (KT)</u>	<u>RADIUS (ft)</u>	<u>DEPTH (ft)</u>	<u>VOLUME (ft³)</u>
MIXED COMPANY-III (Tangent Above)	0.5	58 (68)	13 (13)	6.9 x 10 ⁴ (5.7 x 10 ⁴)
MIDDLE GUST-I (Half Buried)	0.02	49 (40)	17 (17)	6.9 x 10 ⁴ (3.7 x 10 ⁴)
MIDDLE GUST-III (Tangent Above)	0.1	52 (55)	24 (16)	9.9 x 10 ⁴ (5.8 x 10 ⁴)
MIDDLE GUST-IV (Tangent Above)	0.1	43 (36)	15 (26)	4.4 x 10 ⁴ (3.5 x 10 ⁴)

TABLE IV
 CODE PREDICTIONS FOR 5.0 MT RADIATING NUCLEAR BURST AT 1.0 m HEIGHT.
 Empirical Predictions Based on Extrapolations from PPG Data shown in ().

SOURCE	RADIUS	DEPTH (ft)	VOLUME (ft ³)
Ref. 24	196 (700) (1400)	98 (290) (87)	4.0 x 10 ⁶ (2.0 x 10 ⁸)
Ref. 25	213 (950) (900)	183 (400) (120)	1.6 x 10 ⁷ (5.0 x 10 ⁸)
Ref. 26*	337 (950) (1900)	229 (400) (120)	5.2 x 10 ⁷ (5.0 x 10 ⁸)

* degraded material strength; otherwise same as in Ref. 25.

we show instead code predictions vs empirical predictions. The results in the table correspond to a 5.0 MT burst detonated at a height of 1.0 m over two layered geologies which are intended to be representations of Minuteman Missile sites. All three code calculations share a common early time history since they begin with the output from a combined radiation-hydrodynamic code calculation²⁷ for a model weapon (Source 3). The ref. 25 and 26 calculations in Table IV correspond to identical geologies with the difference that the material parameters used in the first were modified in such a way that once-shocked material was assigned a reduced tensile strength.

The empirical values shown in Table IV are "hypothetical data" constructed by means of the Cooper phenomenology described above. Namely, they involve the assumption of cube root scaling, the height-of-burst curve shown in Fig. 3.6 and the geology/material adjustments as determined from craters formed by small HE bursts. Two sets of empirical radius and depth values are shown in Table IV. The upper line corresponds to those appropriate to a "bowl-shaped" crater and the lower to a "disk-shaped" crater as observed at the PPG. The upper values are obtained by extrapolating HE radius/depth curves and the lower by drawing smooth curves through PPG data. One notes that the code predictions are in poor agreement with the "empirical data" and that the two sets of empirical data differ significantly as well.

Not surprisingly the crater is larger in the weakened material (ref. 26 vs ref. 25)--but not much larger. More interesting and perhaps

even encouraging is the larger aspect ratio observed in the weakened case, a result which underlines the critical importance of the strength of materials and fracture criteria employed in the late stage of cratering.

Although much has been said about the apparent inability of codes to predict PPG-like craters, no definitive conclusions can be reached. A detailed review of the calculations shown in Table IV has been made by Kreyenhagen²⁸ and a number of problems uncovered, especially at the Eulerian-Lagrangian boundaries which appear in the codes. We have no original insights but find it hard to believe that the complexities of the PPG coral and coral sand geology, especially the compaction observed in the resurveys, can all be accommodated by a single multiplicative parameter as is assumed when one uses the phenomenology of subsection 3.2 to extrapolate the PPG observations to the code geologies. The simple rules which work for relatively low yield HE shots need not work for large yield bursts.

This page left blank intentionally

IV RADIATIVE COUPLING AND INITIAL IMPULSE

Here we make a unified, albeit crude, calculation that includes both the inner few meters that are directly illuminated by kilovolt X-ray flux from the disassembling warhead and also the next hundred or so meters in radius that are illuminated by radiation scattered in the fireball. Our purposes are (i) to illustrate the relevant physical processes in each of the two regimes, and (ii) to estimate, independently of other investigations, whether fireball coupling may be important.

Because thermal penetration distances are always very small compared with the scale of subsequent ground motions, there is a fairly clean separation between "hot" ($T \gtrsim 10$ eV) and "cold" ($T \lesssim 1$ eV) processes. Heating of the ground and its hydrodynamic blowoff in the fireball is "hot." Groundshock, elasto-plastic response of the rock, and crater-related ground motions are "cold." The "hot" processes are much more rapid in time than the "cold" ones. In first approximation, the coupling between the hot and cold regimes is therefore entirely determined by the impulse per area (as a function of radius) delivered to the cold ground. Zeldovich and Raizer (ch. XII, sec. 13)²⁹ discuss this approximation. In the next approximation, the duration of this impulse might also be relevant, but only when it is longer than the natural duration of the groundshock.

4.1 Source Model

We imagine that each radius r is illuminated for a time $t(r)$ by a blackbody flux of temperature $T(r)$. The functions $t(r)$ and $T(r)$ are chosen to represent a nominal $E = 1 \text{ MT}$ surface burst at a height $L = 1 \text{ m}$. For $r < L$, $t(r)$ is constant:

$$t = \frac{E(\Omega)}{\pi\sigma(T_m)^4 L^2} \quad (r < L) . \quad (4.1)$$

Here $\Omega/4\pi \approx 1/4$ is the solid angle subtended by the zone of radius L , σ is the Stephan-Boltzman constant, and T_m is the effective (not color) temperature of the flux. We adopt $T_m = 1.5 \text{ keV}$ as a standard value, and with the other values already indicated, obtain

$$t(r) = 7 \times 10^{-8} \text{ s} = 70 \text{ ns} . \quad (r < 1 \text{ m}) . \quad (4.2)$$

For $r > 1 \text{ m}$, we match onto a "standard" fireball given in Figure 3 and Table 1 of Brode¹. This becomes our standard source and has $t(r)$ and $T(r)$ as shown in Fig. 4.1.

4.2 Ground Opacity and Radiative Transfer

As an idealization (that is not too inaccurate) we take Kramer's opacity law

$$K = K(\rho, T) = K_{es} \left(\frac{\rho}{\rho_0} \right) \left(\frac{T_B}{T} \right)^{3.5} . \quad T < T_B . \quad (4.3)$$

Here K_{es} is the electron scattering opacity, $K_{es} = 0.2 \text{ cm}^2/\text{g}$,

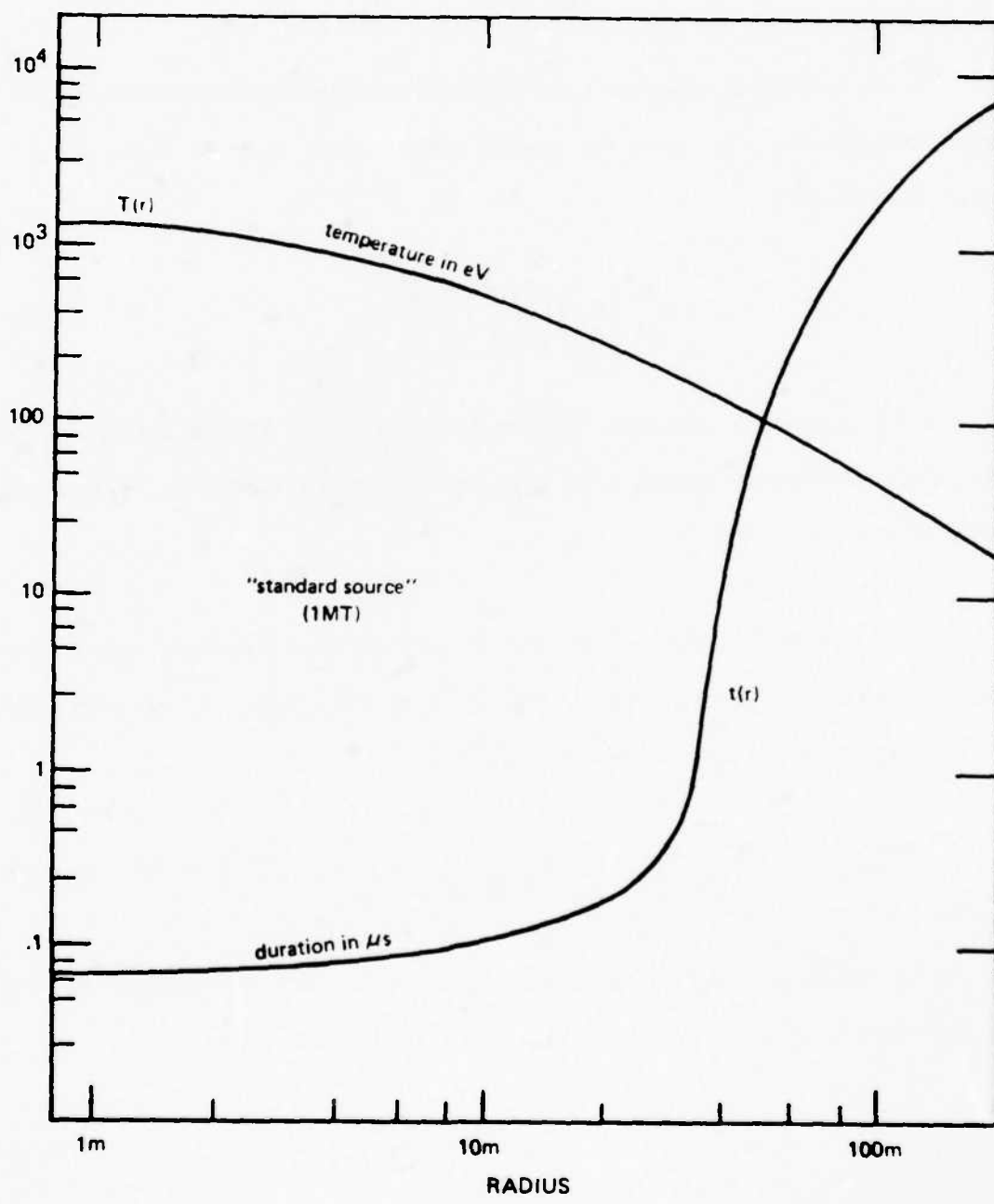


Figure 4.1 THE TIME AND TEMPERATURE FUNCTIONS FOR THE STANDARD 1MT NUCLEAR SOURCE USED IN THIS SECTION.

$\rho_0 = 2 \text{ g/cm}^3$ is ambient density, and T_B is a characteristic burnout temperature. As a standard value we adopt $T_B = 1.5 \text{ keV}$.

We could be somewhat more precise and distinguish the radiation color temperature T_R from the ground temperature T_G by using an effective opacity

$$K = K_{es} \left(\frac{\rho}{\rho_0} \right) \left(\frac{T_B}{T_R} \right)^2 \left(\frac{T_B}{T_\sigma} \right)^{1.5}. \quad (4.4)$$

This would predict a somewhat greater penetration of the radiation in the direct-coupled inner region. We have chosen not to introduce this extra complication.

If radiation and ground are assumed to have the same temperature, then on scales larger than the radiation mean-free-path λ the diffusion of radiation into the ground is governed by

$$\rho C_v \frac{\partial T}{\partial t} - \nabla \cdot \left[\frac{ac}{3K(T, \rho)} \nabla T^4 \right] = 0 \quad (4.5)$$

where a is the radiation constant. It is convenient to rewrite Eq. (4.5) in the form

$$\frac{\partial T}{\partial t} + \frac{4act_s^3 \rho_0}{3K(T_s, \rho_0) C_v \rho^3} \nabla \cdot \left[\left(\frac{T}{T_s} \right)^{6.5} \nabla T \right] = 0. \quad (4.6)$$

In this second form of the equation we have grouped the dimensional quantities into a single diffusion coefficient

$$k \equiv \frac{4acT_s^3\rho_0}{3K(T_s, \rho_0)c_v\rho^3} \quad (4.7)$$

with dimensions (length)²/(time). Here T_s is the temperature applied to the surface, namely $T(r)$ above, and $c_v \approx 6.2 \times 10^7$ erg/g K is the specific heat of the ground matter.

A remark on the dependence of k on ρ is in order at this point. Two powers of ρ appear because we are measuring depth in centimeters rather than grams. The one additional power of ρ comes from Eq. (4.3). So we will have to ask (see below) whether there is appreciable blowoff of matter and reduction of density during the time that the source T_s is applied. Close in, in the kilovolt region, there will be insufficient time for hydrodynamic motion, so we can hold ρ fixed at ρ_0 . As a simple estimate (i.e., which underestimates the coupling in the fireball region) we can take ρ to be fixed at its initial value everywhere.

Treating the density in this way, we see that the depth of penetration of the half-maximum point of energy density is roughly

$$l \approx (tk)^{1/2} \approx 83 \left(\frac{t}{1\mu s} \right)^{0.5} \left(\frac{T_s}{1 \text{ keV}} \right)^{3.25} \text{ cm} . \quad (4.8)$$

Hence the energy deposition per cm^2 is roughly

$$E' \approx \left[\frac{ac^5 C t}{s v K(T_s, \rho_0)} \right]^{1/2} \approx 6.0 \times 10^{16} \left(\frac{t}{1\mu s} \right)^{1/2} \left(\frac{T_s}{1\text{keV}} \right)^{4.75} \text{erg/cm}^2$$

(4.9)

and the impulse per cm^2 generated by the blowoff of the photon-heated layer is roughly

$$P' \approx \left[\frac{ac}{K(T_s, \rho_0)} \right]^{1/2} T_s^{2} t^{1/2} \approx 2.2 \times 10^9 \left(\frac{t}{1\mu s} \right)^{1/2} \left(\frac{T_s}{1\text{keV}} \right)^{3.75}.$$

(4.10)

In Figure 4.2 we plot the function $\ell(r)$ as functions of radius r , using $T(r)$ and $t(r)$ from our "standard" source.

It is interesting to note the appearance of secondary maxima in ℓ at radii of 50 m or so. This maximum occurs because the fireball stagnates for a long time prior to shock breakaway. We now want to see whether this stagnation causes appreciable energy or momentum deposition from the fireball to the ground at these large radii.

4.3 Energy and Impulse Coupled to the Ground

Figure 4.3 plots the energy (solid curves) and blow-off momentum (dashed curves) implied by Eqs. (4.9 and 4.10), with the $T(r)$ and $t(r)$ of our standard source. We plot $r^2 E'$ and $r^2 P'$ vs $\log r$ so that the height of the curve indicates the marginal integrated contribution from

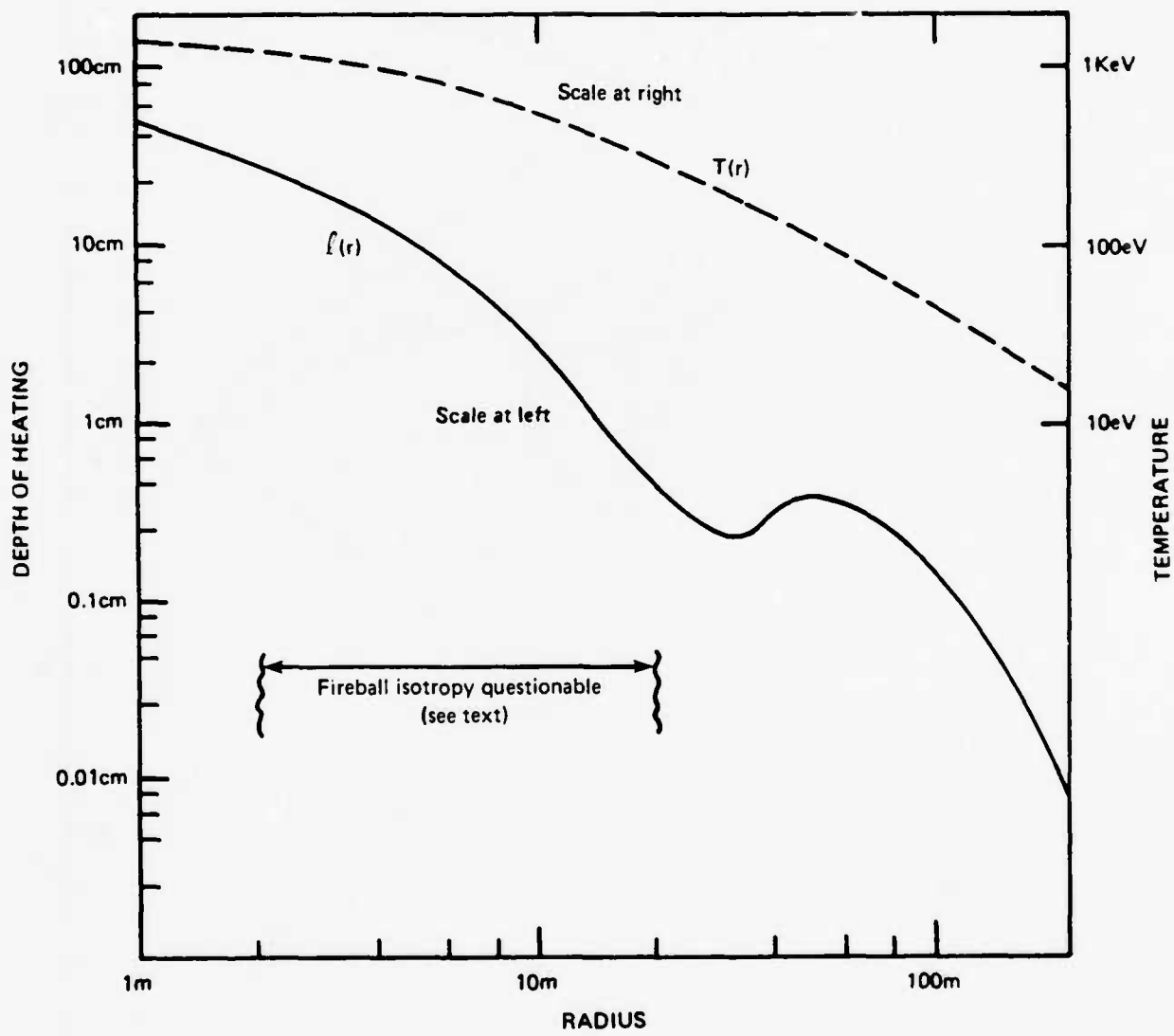


Figure 4.2 THE FIREBALL DEPTH OF HEATING l VS RADIUS r PREDICTED BY EQ. (4.8). ALSO SHOWN FOR CONVENIENCE IS THE TEMPERATURE CURVE FROM FIG. (4.1). FOR THE REASONS DISCUSSED IN THE TEXT, THE MODEL DOES NOT PROPERLY TREAT THE REGION $2m < r < 20m$.

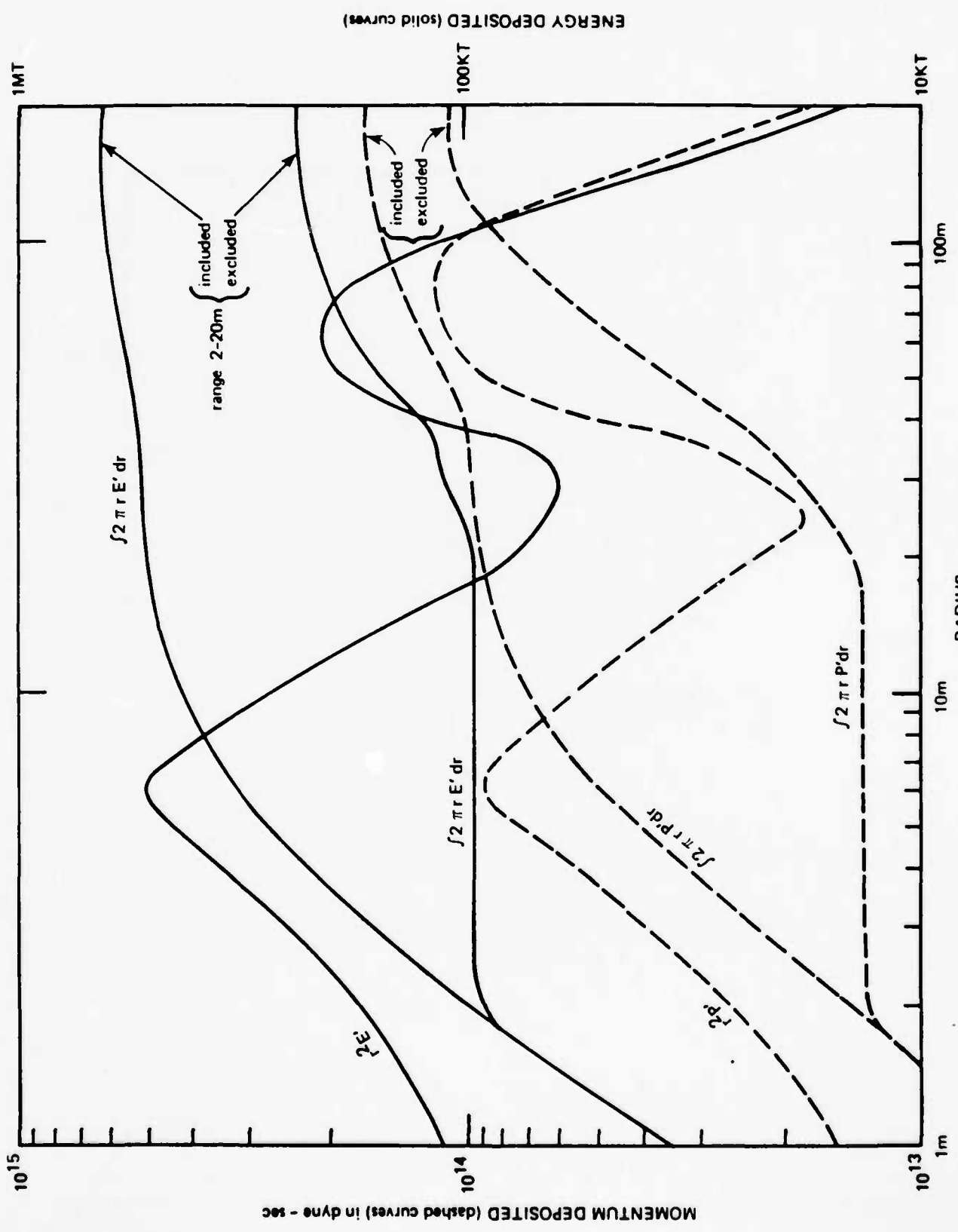


Figure 4.3 ENERGY AND MOMENTUM COUPLED TO THE GROUND ACCORDING TO THE FIREBALL COUPLING MODEL OF THIS SECTION. CURVES FOR THE INTEGRATED CONTRIBUTIONS WITH AND WITHOUT THE QUESTIONABLE INTERMEDIATE REGION ARE SHOWN.

dr . Also plotted for both energy and momentum is an integral curve showing the total energy (in kiloton equivalent) and momentum (in cgs units) deposited inside radius r . In each case, we have computed the integral in two different ways, either including or excluding the contribution predicted by Eq. (4.9) or Eq. (4.10) between 2 m and 20 m radius. This point requires some discussion:

Consider the curve of integrated energy deposition. Inside 1 m radius, our calculation predicts 35 KT (i.e., 3.5% efficiency) deposited into the ground. This number is in line with the detailed calculations^{27,30}, as is our value for the central penetration depth of the radiation. Between 1 m and 2 m, the integral rises to about 9% energy efficiency, which is not too far wrong, considering the crudeness of our treatment. Between 2 m and 20 m, however, it rises to more than 50%. This is certainly spurious, and occurs for a simple reason: the model assumes that the fireball illuminates the ground as a black body, i.e., that the radiation field within the fireball is spatially isotropic. But the scattering length of radiation in the fireball is of order tens of meters. Therefore, until the fireball is of order 20 m, the free-streaming radiation field does not (for the most part) illuminate the ground isotropically. Our effective temperature idealization is fairly good in the first meter or so, where the illumination is from the source directly; it ought also to be good outside of 20 m, where the fireball is optically thick to scattering, but should not be used in between. The choice of 20 m as a cutoff radius is not critical, since the curves in Figure 4.3 show very little additional contribution between 15 m and 40 m.

Between 40 m and 100 m, there is a significant additional deposition, however. Integrated energy rises from 9% (at 2 m and 20 m) to 25% at 200 m if we assume no deposition between 2 m and 20 m. Integrated momentum rises from 1.3×10^{13} dyne-sec to 1.1×10^{14} dyne-sec. While we should not put too much stock in the exact numbers from this model, it seems clear that distant fireball coupling may not be negligible and should be studied with some care. In section V below we compare fireball coupling to the effects of overpressure of the heated air, an effect which may dominate all the effects of energy radiatively coupled into the ground outside of the directly illuminated region.

4.4 Competition Between Hydrodynamics and Radiation Diffusion

In assuming constant ρ in the equation for opacity we may have underestimated the radiation coupling, especially at large radii, so we must now return to the blowoff question.

The rarefaction wave of blowoff propagates into the ground with the (hot) sound speed $v_s \approx (C_v T_s)^{1/2}$, the time t_H at which it catches up with the diffusion wave is roughly

$$v_s t_H \approx (t_H k)^{1/2} \quad (4.11)$$

which gives

$$t_H \approx \frac{T_s^2 ac}{K \rho^2 C_v^2} . \quad (4.12)$$

We must also compute t_2 , defined as the time that it takes to heat a single mean free path λ to temperature T_s , i.e., the time at which the radiation diffusion approximation first starts to be valid:

$$(t_2 k)^{1/2} \approx \lambda \quad (4.13)$$

which gives

$$t_2 \approx \frac{C_v}{K T_a c} \quad . \quad (4.14)$$

Additionally, we need the condition for a rarefaction wave at some temperature $T_1 < T_s$ to propagate through one mean free path in time t_1 before photon heating exceeds the temperature T_1 , i.e.,

$$\lambda \rho C_v T_1 = a c T_s^4 t_1 \quad (4.15a)$$

and

$$\lambda = (C_v T_1)^{1/2} t_1 \quad . \quad (4.15b)$$

Eliminating T_1 between these equations, we get

$$t_1 = \frac{1}{K \rho} \left(\frac{\rho}{a c T_s^4} \right)^{1/3} \quad (4.16)$$

Now eliminating t_1 between Eqs. (4.15a) and (4.15b) and requiring $T_1 < T_s$, we obtain

$$T_s^{5/2} < \frac{\rho}{ac} C_v^{3/2} \approx (150 \text{ eV})^{5/2}. \quad (4.17)$$

What is the meaning of all these conditions? In the $T_{s,t}$ plane they map out the different regimes of competition between photon streaming, diffusion, and blowoff. Figure 4.4 illustrates this. The various boundary lines all meet (approximately) at a critical point

$$T_{\text{crit}} \approx \left(\frac{\rho}{ac} C_v^{3/2} \right)^{2/5} \approx 150 \text{ ev}$$

$$t_{\text{crit}} \approx \frac{C_v^3}{k T_{\text{crit}}^{ac}} \approx 8 \times 10^{-11} \text{ sec}. \quad (4.18)$$

In region (B) of the figure diffusion goes through many mean free paths, then the source turns off, and only subsequently does the rarefaction wave catch up to the diffusion front.

In region (C) diffusion goes through many mean free paths, but the rarefaction catches up while the source is still on. One then goes over to a regime in which a coupled rarefaction-diffusion wave penetrates into the matter faster than $t^{1/2}$, but slower than t .

In region (D), matter starts to blow off even before it reaches the temperature T_s , but it becomes heated to T_s during the subsequent blowoff. In this region a coupled rarefaction-diffusion similarity solution is probably a reasonable approximation during the whole time the source is on.

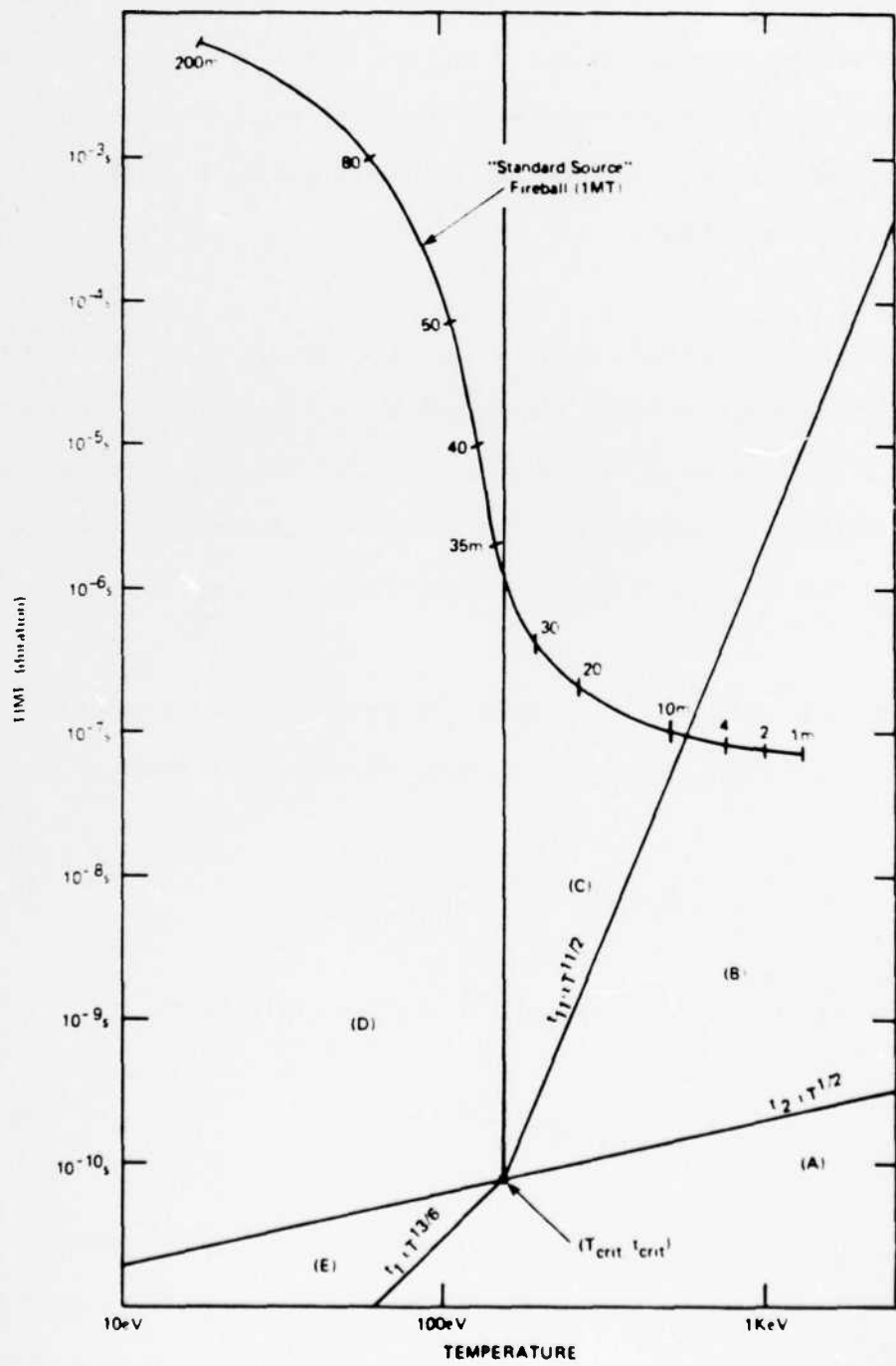


Figure 4.4 THE "TRAJECTORY" OF THE RADIATION - GROUND COUPLING PROBLEM IN TEMPERATURE-TIME SPACE. IN REGION (B) RADIATION DIFFUSES MANY MEAN FREE PATHS BEFORE SOURCE TURNOFF, HYDRODYNAMICS IS NEGLIGIBLE. IN (C) RADIATION DIFFUSES MANY MEAN FREE PATHS BUT HYDRODYNAMIC MOTION CATCHES UP BEFORE SOURCE TURNOFF. IN (D) HYDRODYNAMIC MOTION OCCURS BEFORE GROUND MATERIAL HAS BEEN HEATED TO THE SOURCE TEMPERATURE.

Regions (A) and (E) are never of interest in our problem, since their times are too small. In these regions, the source time is so short that it never heats even a single mean free path to its temperature. In (E), the top mean free path blows off while the source is still on; in (A) the source turns off first.

Also in Figure 4.4, we have indicated the locus of the curve $T(r), t(r)$, parametrized along its length by r in meters. One sees that the curve enters region (D) at $r = 35 \text{ m}$. Thus the distant-fireball coupling, which we have already noted as possibly important, may also be enhanced by the decrease of optical depth with rarefaction.

We can estimate very roughly the possible enhancement as follows: if the penetration was entirely diffusive, it would go to a depth

$$\lambda_{\text{diff}} \sim (t k)^{1/2} \quad (4.19)$$

If it were entirely hydrodynamical, it would go to a depth

$$\lambda_{\text{hydro}} \sim (C_v T_s)^{1/2} t \quad (4.20)$$

The ratio $\lambda_{\text{hydro}} / \lambda_{\text{diff}}$ can be seen (from Eq. 4.11) to be about $(t/t_H)^{1/2}$. Since the true case should be a similarity solution in between these two extremes, the enhancement over the predictions in Fig. 4.3 should be $(t/t_H)^{\alpha/2}$ where $0 < \alpha < 1$. A plausible guess is $\alpha \approx 1/3$ to $1/2$, which (from Figure 4.4) gives enhancement factors of 10 to 100 for energy

and momentum deposition at radii of 50 m. Clearly this is too large, since it would push radiation coupling efficiencies to order unity. We must conclude, however, that a detailed calculation, including details of the blowoff, the change in opacity with blowoff, and radiation transport both in the blown-off material and in the structure of the fireball, is necessary.

This page left blank intentionally

V HYDRODYNAMICS

The purpose of this section is to discuss the hydrodynamic consequences of fireball-coupled energy and momentum, and to describe a simple model for the eventual formation of a crater from the energy and momentum coupled into the ground. These estimates cannot supplant the results of code calculations; rather, their purpose is to identify and explain the dominant physical processes of these code calculations.

5.1 Blowoff

5.1.1 Momentum Amplification

A surface nuclear burst directly heats a very thin layer on the surface of the ground. Close in to the burst the direct radiation heats to a depth of tens of centimeters; in the fireball regime we see from Fig. 4.2 of the preceding section that the depth heated is much less (an accurate number requires a detailed calculation). These surface layers are raised to very high pressure when they are heated, and the recoil of their blowoff delivers a sharp, strong impulse to the ground which sends a shock wave propagating downward.

The one dimensional problem of the propagation of a strong shock from a free surface into a half space is dealt with by Zeldovich and Raizer²⁹. Similarity solutions for these shocks in polytropic gases exist, and take a simple form for $\gamma = 7/5$. This value of γ is a fair

approximation to the properties of ionized gases over a wide range of temperature and density, down to shock pressures of about 1 Mbar. For $\gamma = 7/5$ these authors find the shock speed $u \propto t^{-2/5}$, its distance travelled $x \propto t^{3/5}$, its pressure $P \propto t^{-4/5} \propto x^{-4/3}$, and its impulse per unit area $I \propto t^{1/5} \propto x^{1/3} \propto P^{-1/4}$; other relations may be trivially derived (only one relation is independent). What is striking about these results is the increase in delivered impulse with the depth of penetration of the shock. This phenomenon has been colloquially called "momentum amplification." As the shock penetrates into the ground more and more matter blows off, carrying more and more momentum upward, and producing a correspondingly increasing downward recoil. Equivalently, the energy in the ground is shared by an increasing amount of matter necessarily at a decreasing velocity. The increasing amount of matter involved means that a given amount of energy corresponds to an increasing impulse in the ground (balanced, of course, by the momentum carried by the blown off material). This phenomenon is complicated by the continuing loss of energy from the ground to the blowoff, a loss whose importance depends on the equation of state. For a soft (isothermal) equation of state $\gamma = 1$ and $I \propto t^0$; there is no momentum amplification because the energy in the downward moving ground and its velocity decrease at the same rate. For the hardest polytropic equation of state $\gamma \rightarrow \infty$ and $I \propto t^{0.284}$, slightly more momentum amplification than for $\gamma = 7/5$ because now the energy in downward moving ground decreases very slowly ($\propto t^{-0.074}$) while the velocity decrease $u \propto t^{-0.358}$ is still rapid.

Close in to the burst the deposition of radiative energy is rapidly varying horizontally, so the ground motion is a two dimensional problem. Fortunately, this problem is well calculated by existing codes, and is not controversial. There is more argument about the fate of the coupled energy and momentum in the fireball region, where the motion is very close to slab-symmetric, but where the initial deposition is in such a thin layer that numerical calculation may be tricky. Although millimeters of solid ground are eventually heated, the first mean free path, which is the thickness of the initial blowoff in most of the fireball, is only about $10\mu\text{m}$ thick (see Fig. 4.2). It is here that we wish to discuss the momentum amplification problem using the results of Zeldovich and Raizer.

The inner parts of the fireball ($r < 35 \text{ m}$) are in region C of Fig. 4.4 of the preceding section. Initially the fireball heats at least one optical depth to its effective temperature $T > 150 \text{ eV}$. At solid density this hot ground has a pressure $\sim 100 \text{ Mbar}$, and the equation of state is that of a gas. Under adiabatic conditions it may be reasonably described with a polytropic equation of state $P \propto \rho^\gamma$, where γ lies between 1 and $5/3$, depending on how rapidly the degree of ionization is varying with temperature, and hence on entropy. We shall use $\gamma = 7/5$ throughout.

Even for the most favorable equations of state momentum amplification is a slow process. It is limited by the range in pressure over which the matter retains its polytropic equation of state. For shock pressures below 1 Mbar the matter is not in a vapor or plasma phase upon

unloading, but rather is a fractured solid, the hydrodynamics of which are much closer to that of an incompressible fluid than that of a polytropic gas. A pressure of 1 Mbar is the lower bound on the region of validity of the momentum-amplifying blowoff, so the total amplification for $\gamma = 7/5$ is $(100)^{1/4} \approx 3$. In practice momentum amplification is even smaller than this for two reasons: (1) porosity and microstructure (sand, snow, vegetation, etc.) in the uppermost layers of ground reduce the density, and hence the pressure, at which the amplifying process begins and (2) no momentum amplification applies to energy delivered after the initial rarefaction catches up to the radiation diffusion front, because such energy is not deposited in solid-density, high pressure (100 Mbar) matter.

Beyond 35 meters (standard fireball), the fireball radiation is softer ($T < 150$ eV), and, as discussed in the preceding section, penetrates less efficiently into the ground. Most of the fireball coupling occurs in the range between 50 and 100 meters, where $T < 100$ eV. No portion of the ground is ever heated to the fireball temperature before it is cooled by rarefaction. Peak pressures are then much lower than regions for which $T > 150$ eV, partly because the fireball temperature is lower and partly because the ground does not reach even this reduced temperature. In such regions there is reduced opportunity for momentum amplification.

The fundamental reason why momentum amplification over most of the fireball region is insignificant may be seen from the time scales in Fig. 4.4. For $T < 150$ eV the fireball duration exceeds t_1 , the time for the rarefaction to catch up with the heating front, by several orders of

magnitude. Only a $10\mu\text{m}$ thick skin is heated during the first interval t_1 . For the case $T > 150 \text{ eV}$ which applies only over a small region the fireball duration should be compared to t_H ; the inequality is still large. Energy deposited after the brief initial time t_1 , (or t_H), leads to little or no momentum amplification, because it is deposited in low density blowoff at pressures far below the peak of 100 Mbar. This later time includes more than 99.9% of the fireball deposition outside 30 m, the beginning of the fireball regime. Even the existence of the initial transient is dubious, because the front of a real fireball does not produce an instantaneous jump in its radiation field, but has some finite width.

5.1.2 Air Tamping

After the rarefaction front catches up to the thin, initially fireball-heated, surface layer, a coupled rarefaction-thermal front penetrates into and ablates the ground. As discussed in the preceding section, it is hard to calculate simply with pencil and paper the progress of the front and its depth of penetration, but it is tractable on a computer. Some general considerations are easy to establish, however. The ablated matter is heated to the fireball temperature, but only after it rarefies. The maximum pressure is far below the 100 Mbar value which solid density matter has at fireball temperature, so that the maximum possible momentum amplification is reduced below the bound of 3; it cannot be much more than unity. If the blowoff were into vacuum the maximum density (and hence maximum pressure) in the flow would be a steadily decreasing function of time, as a thickening layer of ablated material built up between the radiation source and the solid ground. Reality is different (until we

fight wars on the Moon). The ground is covered with air at fireball temperature. At a density of 10^{-3} g/cm³ and at fireball temperatures, air is multiply ionized (generally five times for nitrogen and six times for oxygen) and has a pressure of $\sim 10\text{-}30$ Kbar. Once the ground blowoff has rarefied to the same density as air the pressures of the two materials are nearly equal (both are multiply ionized, and have similar mean Z). This happens rather quickly in a relaxation time t_r of about ρ_g/ρ_{air} times the initial rarefaction time t_1 or t_H . At the 100 eV point in our standard fireball, $t_r \sim 10^{-7}$ which corresponds to about 10^{-3} of the fireball duration. Then the air decelerates the expanding front of the blowoff. After a time equal to a few times t_r , pressure pulses are exchanged through the blowoff from air to ground and back again, and as transient effects die away the blowoff air and upper portion of the dense ground settle down to a nearly isobaric condition. The reason for this is the short relaxation time for pressure through the thin layers between the semi-infinite atmosphere (already isobaric) and the semi-infinite dense ground. After these initial transients, all other properties of the ablating flow change slowly. Eventually (in $10^{-4} - 10^{-3}$ s) this steady state is brought to an end by the turning off of the fireball, or the progress inward of a rarefaction in the air from its upper surface. Until then, the fireball and ablating surface act as a simple pressure boundary condition on the ground, and a planar shock propagates downward. Because this shock is weak (the overpressure is tens of kilobars) it produces negligible compression, no blowoff, and no vaporization.

It may be seen from Fig. 5.1 that the "airslap" contribution to ground impulse we have just described appears to be dominant (remember, though, that for the close in coupling momentum amplification may be a factor of ~ 10). Particularly striking is the fact that the delivered impulse is still rapidly increasing at 200 meters, the limit of available fireball parameters. What limits this impulse?

Airslap is large because area and dwell time both increase rapidly outward in the fireball, while temperature decreases only moderately. Eventually though, and not too far beyond 200 m, the fireball reaches its maximum extent; beyond this point its dwell time drops abruptly to zero, and there is no fireball. There is still some airslap from shocked air, but its overpressure is negligible. A second limiting factor enters at the outer edge of the fireball. The air overpressure, which is about 10 Kbar at 200 meters, is dropping. Once it drops below the crushing strength of rock (one or a few Kbar) the shocked rock can unload elastically, and the delivered impulse does not contribute to cratering. Because of the large contribution to impulse coupling of the outer edge of the fireball, it is important that computer codes treat the late time, low pressure regime well if accurate results are to be obtained.

5.2 Incompressible Hydrodynamics

Under the fireball is a weak, downward propagating shock. Its peak pressure is much less than 1 Mbar, so it produces very little compression. It travels at a velocity very close to the compressional sound speed v_s ($v_s \approx$ few km/s); the shocked material has a subsonic

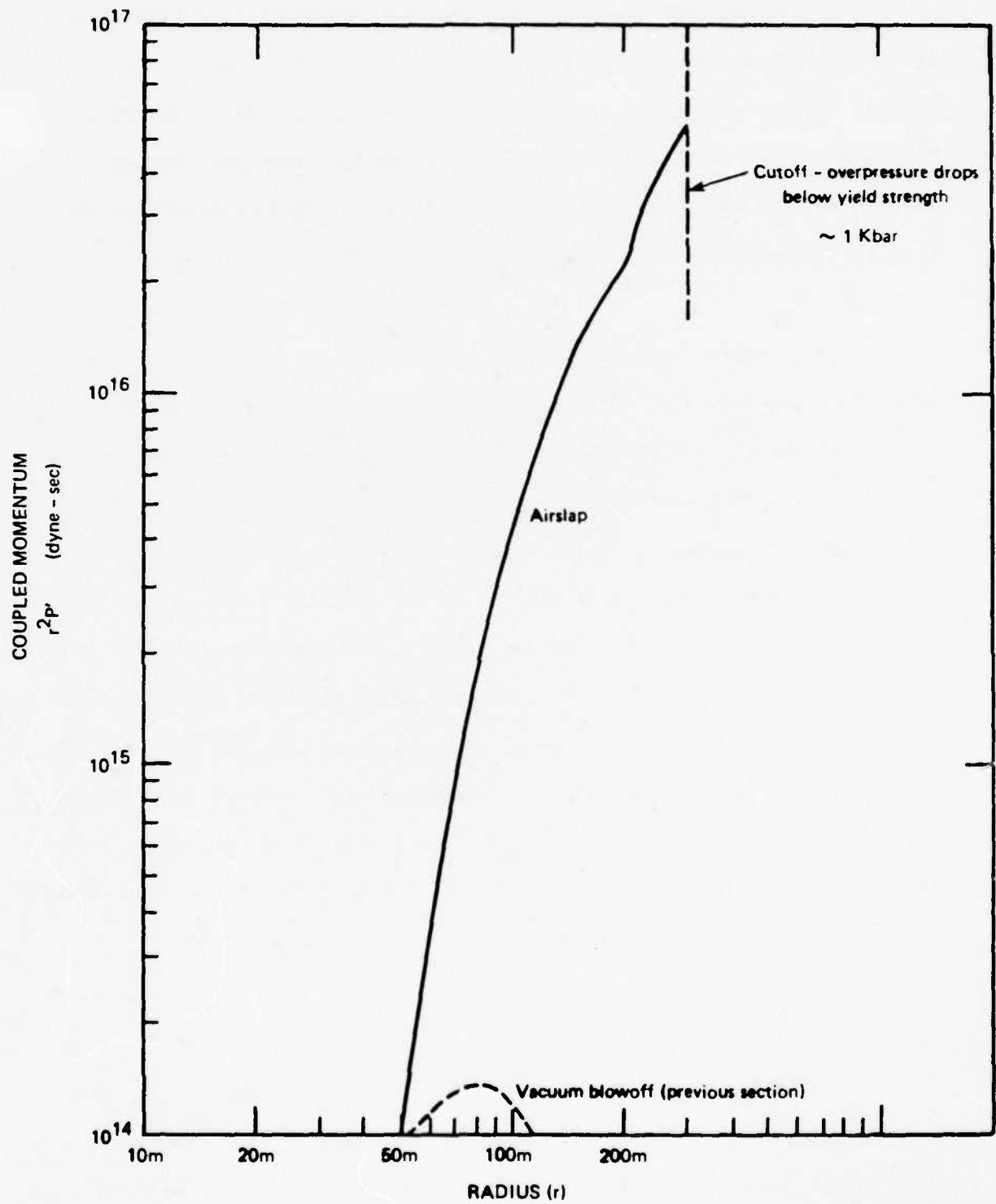


Figure 5.1 CONTRIBUTIONS TO THE MOMENTUM IMPULSE GIVEN TO THE GROUND FROM THE RADIATION INDUCED VACUUM BLOWOFF DESCRIBED IN THE PRECEDING SECTION AND THE AIRSLAP DISCUSSED IN THIS SECTION.

downward velocity of $v \approx \frac{P}{\rho v_s}$, which is ~ 100 - 300 m/s. These conditions continue, the shock propagating downward, until the fireball ceases and the surface pressure relaxes to zero. Then a rarefaction follows the shock leaving in its wake matter at rest, but displaced downward. In slab symmetry the rarefaction would chase the shock deep into the earth, very slowly attenuating it. In the real world the fireball is of finite horizontal extent. The shock propagates sideways in addition to downward, and as it propagates horizontally the free surface is a continuous source of rarefactions. When rarefactions interact they produce a state of net tension in which the rock fragments. The final displacement of this loose material creates the crater.

If the eventual crater is larger than the fireball, as we expect, its size may be roughly estimated. All of the momentum delivered to the ground, whether close in to the burst or out at the limits of the fireball, may be combined into a single downward impulse concentrated at one point. The details of compressible hydrodynamics near the burst and at the surface under the fireball (pressures over 1 Mbar, or temperatures over 1 eV) are ignored--all that matters is the impulse they deliver into a much larger volume which undergoes essentially incompressible flow. Because the stresses far exceed the yield strength of rocks we may assume that the flow is hydrodynamic, until the outer limits of the cratered volume are reached. As sketched in Fig. 5.2 the downward impulse I is spread over a steadily widening area. Approximately we can write

$$I = PR^2 \Delta t \quad (5.1)$$

solution is probably a reasonable approximation during the whole time the source is on.

IV-12

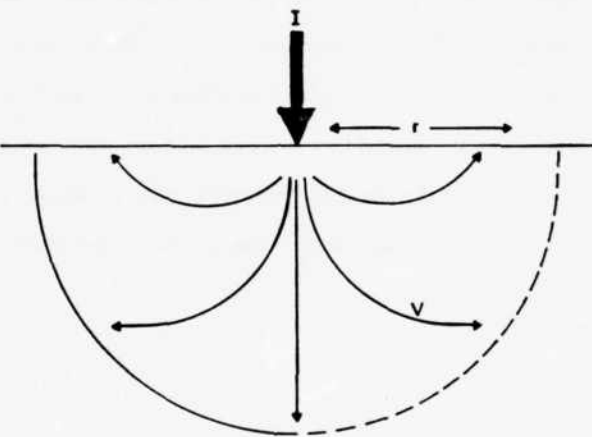


Figure 5.2 THE INITIAL DOWNWARD IMPULSE TRANSFERRED TO THE GROUND SPREADS OVER A WIDENING AREA BY HYDRODYNAMIC MOTION WHICH IS WELL APPROXIMATED BY INCOMPRESSIBLE FLOW.

V-10

where P is a typical pressure in the flow and Δt its duration. Then, similarly approximately, $\Delta t = R/v$, where v is a typical velocity, and M is the mass swept up in the flow

$$v = I/M = I/\rho R^3 . \quad (5.2)$$

The size of the cratering flow is thus estimated by

$$R = I^{1/3}(\rho P)^{-1/6} . \quad (5.3)$$

As the flow spreads out, and the momentum is spread over an increasing mass of crushed and fragmented rock, kinetic energy is lost to internal and external friction and to fracture energy. This process terminates when P reaches the strength of the rock; lower stresses are carried away by elastic waves. Then the final crater size is approximately given by $R \approx I^{1/3}(\rho P)^{-1/6}$; beyond this radius the rock is unfractured. This estimate is crude, and is particularly bad for unconsolidated materials like sand whose strength is strongly dependent on loading. As before, our estimates are not meant as a substitute for computer calculations, but rather as a simple model to assist understanding.

This page left blank intentionally

VI CONCLUSIONS AND RECOMMENDATIONS

- (1) We have found the cratering problem to be a complex one indeed. Its intrinsic complexity is exacerbated by the poorly documented experimental data for the few existing surface bursts of modern, radiating nuclear weapons and by the small overlap in source configurations, material descriptions, etc., which have been employed in computer studies. None of this is new to the workers in the field who indeed seem to share the same frustrations. Further efforts to compare, contrast and refine theoretical calculations are strongly encouraged.
- (2) The apparent success of computer predictions for crater formation by high explosives (HE) in simple geologies is highly relevant since one must work through similar hydrodynamic, elasto-plastic and rock fracture processes in the nuclear case as well. If the HE success is real then it follows that if one can calculate accurately the energy and momentum configuration in the ground at the end of the radiation era, one ought to be able to carry the remainder of the calculation through to a reliable result for a nuclear crater. Comparisons of code and centrifuge HE cratering experiments have not yet been done but would provide valuable checks on numerical calculations in well defined situations.
- (3) The crude model of radiation coupling we develop in section IV gives order of magnitude confirmation of the predictions^{27,30} that only a small fraction (few percent) of the direct radiation is coupled into the

ground. This directly coupled energy is concentrated in a small region ($r < 5$ m) and occurs during $t \lesssim 100$ ns for a 1 MT burst. The predicted depth to which this radiation penetrates is also qualitatively reproduced by our model ($d \approx 60$ cm).

(4) The radiation model of section IV also indicates that the total (integrated over area) energy which is coupled from the fireball into the ground at large distances from the source ($r \approx 40-200$ m), is comparable to the directly coupled energy. This comes about in spite of the lower fireball temperature because of the long duration of the fireball at these radii ($t \approx 10^{-5} - 10^{-2}$ s) and the quadratic increase of area with radius. The initial impulse generated by the fireball coupling is also predicted to be comparable to the initial impulse generated in the close-in region by the directly coupled radiation. The depth of the fireball heating is, however, very small. Precise values depend on the solution of a combined hydrodynamic blowoff-radiation diffusion problem we have not undertaken. At $r = 50$ m the heating depth is expected to lie somewhere between 0.4-4 cm and to decrease to 0.01-0.1 cm at $r = 200$ m.

(5) We are not sure if the net effect of fireball coupling will be sizable enough to have a significant influence on final crater size or configuration. We believe, however, just as for the problem of direct radiation coupling, that the correct answer is fully within the grasp of present theoretical knowledge and computer capability.

(6) In an effort to effect a convergence among the various numerical code results for the radiation coupling, we recommend a series

of bench mark calculations. These might be designed as follows: In order to separate the complications of geometry from the radiation/hydrodynamic issues of primary interest, a series of one dimensional calculations could be undertaken which correspond to a wide variety of radiation temperatures (or spectral conditions as appropriate) and time durations. The range of these parameters should cover conditions from those appropriate to the direct radiation all the way to those appropriate to typical fireball conditions at late times. In this way, one could develop a clear sense of the various depth and time scales involved in all parts of the cratering problem at all radii. This knowledge could then be used to assure that nothing important is being lost in the full geometry, realistic crater calculations.

(7) As part of the radiation studies we recommend that considerable attention be given to the sensitivity to height of burst. Since it may very well be that modern nuclear weapons do indeed produce small craters, the dependence on height of burst may be complex. Calculations over a wide range of heights are needed. In doing this work, the source should be characterized in simple terms rather than including complex details of design and configuration.

(8) When satisfactory convergence has been obtained on the radiation coupling calculations, and especially if the results settle on small efficiencies of cratering, one ought then to go back and trace through the fate of the other (small) weapon energy releases--case debris, neutron emission, etc.

(9) It may be particularly important to accurately calculate the effects of airslap in the outer parts of the fireball, and to understand the yield properties of the undisturbed ground at stresses not far above its elastic limit.

(10) Since it seems to be clear that the mechanisms of coupling and the resulting spatial distributions for modern nuclear weapons are quite different from those of high explosive bursts, the same scaling laws need not apply to both. It could therefore be very misleading to apply the empirical scaling laws which have been extracted from the extensive HE data base to nuclear weapon bursts.

(11) There is evidently a considerable disagreement over the appropriate description of material properties and yield criteria which go into cratering calculations and the level of detail which is necessary. It would be valuable to have some simplified reference calculations which would indicate the sensitivity to various descriptions.

(12) We have little to say about the craters which were produced during testing in the Pacific Proving Ground (PPG). The actual device environments are so unknown and the crater modifications (wave washing, slumping, etc.) which may have occurred after the burst are so uncertain, that the PPG nuclear data may have been rendered essentially useless. Applications to the PPG craters of scaling laws, which themselves have very limited verification, should be treated with great caution.

REFERENCES

1. H.L. Brode, "Review of nuclear weapon effects,"; Annual Review of Nuclear Science, 18, 153, (1968).
2. C.P. Knowles and H.L. Brode, "The theory of cratering phenomena, an overview," in Impact and Explosion Cratering, D.J. Roddy, R.O. Pepin and R.B. Merrill (eds.), (1977), p. 869.
3. A. J. Chabai, "On scaling dimensions of craters produced by buried explosives," Geophys., Res. 70, 5075 (1965). See also D. Divoky, "Comment on a paper by A. J. Chabai," Journal of Geophys., Res. 71, 2691, (1966).
4. L. J. Vortman, "Craters from surface explosions and scaling laws," Geophys., Res. 73, 4621 (1968); B. K. Crowley, "Scaling criteria for rock dynamic experiments" in Symposium on Engineering with Nuclear Explosives 1, (1970), p. 545.
5. R. M. Schmidt and K.A. Holsapple, "Theory and experiments on centrifuge cratering," Geophys. Res. 85 235 (1980).
6. R. M. Schmidt and K.A. Holsapple, "A material strength model for apparent crater volume," Proc Lunar and Planet Sci. Conf. 10th, 1979 p. 2757, and references therein.
7. A. J. Piekutowski, "Laboratory-scale high explosive cratering and ejecta phenomenology studies, AFWL-TR-72-155, April 1974; "A comparison of cratering effects for lead azide and PETN explosive charges," AFWL-JR-74-182, May 1975, Air Force Weapons Lab. Albuquerque, N.M.
8. See, for example, the discussion given in ref. (1).
9. R.M. Schmidt and K.A. Holsapple, "Centrifuge simulation techniques," Status Report, DNA001-78-C-0149. Dec. 1979.
10. R. M. Schmidt and K.A. Holsapple, "Centrifuge crater scaling experiment II: Material Strength effects," DNA Report 4999Z, May 1979.
11. R. M. Schmidt and K.A. Holsapple, "Centrifuge crater scaling experiment III: HOB/DOB effects," DNA Report (in preparation), 1979.
12. R.M. Schmidt, "Centrifuge simulation of the Johnie Boy 500 ton cratering event," Proc. Lunar Planet Sci. Conf. 9th (1978), p 3877.

13. R.T. Allen, unpublished calculations based on the nuclear coupling calculations of D. Maxwell, J. Reaugh and B. Gerber, "Johnie Boy crater calculations," DNA Report 3048F (1973) and D.L. Orphal, Calculations of explosion cratering - I: the shallow buried nuclear detonation Johnie Boy," in Impact and Explosion Cratering, D.J. Roddy, R.O. Pepin and R.B. Merrill (eds.), (1977), p.897.
14. H.F. Cooper, "Estimates of crater dimensions for near surface explosions of nuclear and high-explosive sources", RDA-TR-2064-001, Sept, 1976, R. and D. Associates.
15. H.F. Cooper and F.M. Sauer, "Crater-related ground motions and implications for crater scaling," in Impact and Explosion Cratering, D. J. Roddy, R.O. Pepin and R.B. Merrill (eds.), (1977), p. 1133.
16. R.E. Crawford, C. J. Higgins and E.H. Bultmann, "The Air Force Manual for Design and Analysis of Hardened Structures," AFWL-TR-74-102, Oct. 1974 Air Force Weapons Laboratory.
17. "DNA Nuclear Weapons Effects Manual," EM-1, revised 1979.
- 17a. J. R. Lilley, "The Systematics of Near-Surface-Burst Nuclear Excavation Data", Unpublished Report, Jan. 1977, Los Alamos Scientific Laboratory (unpublished).
18. This is reviewed in detail in ref. (14).
19. B.L. Ristvet, et al., "Geologic and geophysical investigations of the Eniwetok nuclear craters," AFWL-TR-77-242, Sept. 1978, Air Force Weapons Laboratory.
20. G.W. Ullrich, unpublished. See ref. (2).
21. D.L. Orphal, ref. (13).
22. G. Lalongo, "Prediction calculations for the Mixed Company-III event," DNA - 3206T (1973), Shock Hydrodynamics Division, Whittaker Corporation.
23. S. Schuster, "Results of pre-test prediction calculation of Middle Gust I,II and III, (1973), Applied Theory, Inc.
24. G. Lalongo, S.W. McDonald and J.B. Reid, "A two dimensional calculation of large burst phenomenology," DNA 3397 F (1974), Shock Hydrodynamics International.

25. D. L. Orphal, D.E. Maxwell, J.E. Reaugh and W.F. Borden, "A computation of cratering and ground motion from a 5 MT nuclear surface burst over a layered geology," DNA 3711 F (1975) Physics International Company.
26. R.P. Swift, "Material strength degradation effect on cratering dynamics," in Impact and Explosion Cratering, D.R. Roddy, R.O. Repin and R.B. Merrill (eds.), (1977), p. 1025.
27. "Source 3 Calculation," (1978) Systems Science and Software (unpublished).
28. K.N. Kreyenhagen, presentation at the DNA Cratering Working Group Meeting, Marina Del Rey, Oct. 1979.
29. Y.B. Zeldovich and Y. P. Raizer, Physics and Shock Waves and High-Temperature Hydrodynamic Phenomena, Vol II, Academic Press, (1967).
30. "Nuclear Explosion HOB Study-I," SAND-78-0546 (1978), Sandia Laboratories (unpublished).

This page left blank intentionally

DISTRIBUTION LIST

<u>ORGANIZATION</u>	<u>NO. OF COPIES</u>	<u>ORGANIZATION</u>	<u>NO. OF COPIES</u>
Dr. Alf Andreassen Technical Director, OPNAV-095T1 Room 5D616, The Pentagon Washington, D.C. 20350	1	Dr. Edward Harper OPNAV-021T Room 4D544, The Pentagon Washington, D.C. 20350	1
CDR Paul Brouer NFOIO Detachment, Suitland 4301 Suitland Road Washington, D.C. 20390	1	Dr. George A. Keyworth Director Office of Science & Tech. Policy Executive Office of the President Washington, D.C. 20500	1
CDR Robert Cronin Dep Asst Secy Navy (C ³ I) Office of Asst Secy Navy for RE&S The Pentagon, Rm 4E749 Washington, D.C. 20350	1	Mr. Ray Leadabrand SRI International 333 Ravenswood Avenue Menlo Park, CA 94025	1
Defense Technical Information Center Cameron Station Alexandria, VA 22314	2	SRI/MP Reports Area G037 333 Ravenswood Avenue Menlo Park, CA 94025 ATTN: D. Leitner	2
The Honorable Richard DeLauer Under Secretary of Defense (R&E) Office of the Secretary of Defense Room 3E1006, The Pentagon Washington, D.C. 20301	1	Mr. Barry Leven NISC/Code 20 4301 Suitland Road Washington, D.C. 20390	1
Dr. David D. Elliott SRI International 333 Ravenswood Avenue Menlo Park, CA 94025	1	Dr. Donald M. LeVine SRI International 1611 N. Kent Street Arlington, VA 22209	3
Dr. Henry M. Foley Department of Physics Columbia University New York, NY 10027	1	Director National Security Agency Fort Meade, MD 20755 ATTN: Mr. Robert Madden, R/SA	1
Director National Security Agency Fort Meade, MD 20755 ATTN: Mr. Richard Foss, A052	2	Mr. John Meson DARPA 1400 Wilson Boulevard Arlington, VA 22209	1
Dr. Robert Fossum, Director DARPA 1400 Wilson Boulevard Arlington, VA 22209	2	Dr. Julian Nall P.O. Box 1925 Washington, D.C. 20013	2

<u>ORGANIZATION</u>	<u>NO. OF COPIES</u>	<u>ORGANIZATION</u>	<u>NO. OF COPIES</u>
Prof. William A. Nierenberg Scripps Inst. of Oceanography University of California, S.D. La Jolla, CA 92093	1	Director Defense Nuclear Agency Washington, D.C. 20205 ATTN: DDST ATTN: STSP ATTN: SPSS ATTN: TITL	1 1 2 4
Dr. H. Alan Pike DARPA/DEO 1400 Wilson Boulevard Arlington, VA 22209	2	Defense Technical Information Center Cameron Station Alexandria, VA 22314 ATTN: DD	12
Dr. Eugene Sevin Defense Nuclear Agency Washington, D.C. 20305	2	Director U.S. Army Engr Waterways Exper Station P.O. Box 631 Vicksburg, MS 39180 ATTN: J. Zelasko	1
Dr. Joel A. Snow Senior Technical Advisor Office of Energy Research, U.S. DOE, M.S. E084 Washington, D.C. 20585	2	Air Force Weapons Laboratory, AFSC Kirtland AFB, NM 87117 ATTN: NTES-C R. Henny ATTN: NTES-G R. Couch ATTN: NTES J. Lee	1 1 1
Dr. Al Trivelpiece Director, Office of Energy Research, U.S. DOE M.S. 6E084 Washington, D.C. 20585	1	VELA Seismological Center 312 Montgomery Street Alexandria, VA 22314 ATTN: G. Ullrich	1
Dr. James P. Wade, Jr Prin. Dep. Under Secretary of Defense for R&E The Pentagon, Room 3E1014 Washington, D.C. 20301	1	Department of the Interior U.S. Geological Survey 2255 North Gemini Drive Flagstaff, AZ 86001 ATTN: D. Roddy	1
Ms. Alice Wright SRI International 333 Ravenswood Avenue Menlo Park, CA 94025	1	Applied Research Associates, Inc. New England Division Johnson Hill Road, RFD #1 South Royalton, VT 05068 ATTN: S. Blouin	1
Commander Field Command Defense Nuclear Agency Kirtland AFB, NM 87115 ATTN: FCTT W. Summa ATTN: FCTK B. Ristvit	1		

<u>ORGANIZATION</u>	<u>NO. OF COPIES</u>	<u>ORGANIZATION</u>	<u>NO. OF COPIES</u>
Boeing Co. P.O. Box 3999 Seattle, WA 98124 ATTN: K. Holsapple ATTN: R. Schmidt	1 1	Los Alamos National Scientific Lab P.O. Box 1663 Los Alamos, NM 87545 ATTN: B. Killian ATTN: C. Keller ATTN: M/S632 T. Dowler ATTN: M. Henderson ATTN: J. Lilley	1 1 1 1 1
California Institute of Technology Seismological Laboratory Pasadena, CA 91125 ATTN: T. Ahrens	1	Pacific-Sierra Research Corp. 1456 Cloverfield Blvd. Santa Monica, CA 90404 ATTN: L. Schlessinger ATTN: H. Brode	1 1
California Research & Technology, Inc. 6269 Variel Avenue Woodland Hilld, CA 91364 ATTN: S. Schuster ATTN: K. Kreyenhagen	1 1	Pacifica Technology P.O. Box 148 Del Mar, CA 92014 ATTN: R. Allen	1
California Research & Technology, Inc. 4049 First Street Livermore, CA 94550 ATTN: D. Orphal	1	Physics International Co. 2700 Merced Street San Leandro, CA 94577 ATTN: J. Thomsen ATTN: F. Sauer	1 1
University of California Department of Astronomoy Los Angeles, CA 90024 ATTN: J. Katz	1	R & D Associates P.O. Box 9695 Marina Del Rey, CA 90291 ATTN: R. Port ATTN: C. MacDonald ATTN: J. Lewis ATTN: P. Haas	1 1 1 1
Energy Systems, Inc. P.O. Box 6065 Anchorage, AK 99502 ATTN: W. Ogle	1	Sandia National Lab P.O. Box 5800 Albuquerque, NM 87185 ATTN: A. Chabai ATTN: L. Vortman	1 1
University of Illinois Physics Department Urbana, IL 61801 ATTN: J. Sullivan	1	Science Applications, Inc. P.O. Box 2351 La Jolla, CA 92038 ATTN: H. Wilson ATTN: M. McKay	1 1
Lawrence Livermore National Lab P.O. Box 808 Livermore, CA 94550 ATTN: D. Clark ATTN: L-10 H. Kruger ATTN: W. Crowley ATTN: D. Burton	1 1 1 1		

<u>ORGANIZATION</u>	<u>NO. OF COPIES</u>	<u>ORGANIZATION</u>	<u>NO. OF COPIES</u>
Systems, Science & Software, Inc. P.O. Box 1620 La Jolla, CA 92038 ATTN: C. Dismukes ATTN: K. Pyatt	1 1	Weidlinger Assoc., Consulting Engineers 110 E. 59th Street New York, NY 10022 ATTN: I. Sandler	1

END